Supplementary Information For:

Leveraging Ordered Voids in Microporous Perovskites for Intercalation and Post-Synthetic Modification

Connor W. Dalton, Paige M. Gannon, Werner Kaminsky, and Douglas A. Reed*

Department of Chemistry, University of Washington, Seattle, WA 98195 USA

Table of Contents:

1. Experimental

General Materials and Methods. Reagents and solvents were purchased from commercial sources (Millipore Sigma, TCI America, STREM, Fisher, Oakwood Chemical) and used without further purification unless otherwise noted. DMSO-d_6 was purchased from Millipore Sigma and used as purchased. NMR spectra were acquired on Bruker 300 or 500 MHz spectrometers and ^{1}H NMR signals were referenced to the residual DMSO-d_6 peak. Mass spectrometry of APOSSCl_8 and APOSSBr_8 were collected on a Waters QuattroMicro API instrument in negative ion mode. Powder X-ray diffraction data were collected on a Bruker D2 PHASER benchtop diffractometer. Indexing and Pawley refinement of PXRD data was conducted on TOPAS V6. FTIR spectra were collected on a Perkin Elmer Frontier FTIR instrument (1 cm^{-1} resolution) in both ATR and transmission modes. For transmission mode measurements, samples were prepared as 0.5 wt% KBr pellets. DRS spectra were collected on a Shimadzu 3600 i Plus spectrometer and converted to absorbance using the Kubelka-Munk equation. DRS samples were prepared as 5 wt% $BaSO_4$ powders and the scattering factor in the Kubelka-Munk was assumed to be dominated by scattering from the $BaSO_4$. $Cu(SCN)_2$ was prepared according to a literature procedure.[1]

Synthesis of APOSSCl_8. Adapted from Gravel *et al.*[2] To a 5 L 2-neck flask loaded with a stir bar was added 870 mL of MeOH and the headspace was purged with N_2 overnight. To the MeOH was added 3-aminopropyltriethoxysilane (100 mL, 0.43 mol) and concentrated HCl (147 mL). The reaction was stirred for 15 minutes after which the reaction sat with no stirring for 2 weeks. The resultant white powder was isolated through vacuum filtration, washed with cold MeOH (10 x 10 mL). The product was dried *in vacuo* to yield a white powder (20 g,17 mmol, 32%). ^{1}H NMR (300 MHz, DMSO-d_6, 298 K): δ = 8.16 (24H, br), 2.79 (16H, br), 1.73 (16H, br), 0.74 (16H, br) ppm.

Synthesis of APOSSBr_8. To a column loaded with Amberlight IR 400 (Cl) was added deionized H_2O (150 mL), aqueous KBr solution (190 mL, 1 M), deionized H_2O (400 mL), and MeOH (100 mL) sequentially. APOSSCl_8 (0.49 g, 0.4 mmol) dissolved in 5 mL of 95% v/v MeOH:H_2O solution was added to the column along with MeOH (250 mL). The fractions were collected and concentrated to ~10 ml *in vacuo* and the column was regenerated using the prior sequence of solvents. The process was repeated an additional 2 times before the solvent was removed from the final fraction *in vacuo* to yield a white solid (0.56 g, 0.37 mmol, 92%). ^{1}H NMR (300 MHz, DMSO-d_6, 298 K): δ = 7.89 (24H, br), 2.81 (16H, br), 1.69 (16H, br), 0.72 (16H, br) ppm.

Synthesis of (APOSS)$[CuCl_4]_4$. Adapted from Kataoka *et al*.[3] To a beaker containing ~50 mL of EtOH was added a solution of APOSSCl_8 (200 mg, 0.17 mmol) and $CuCl_2{\cdot}2H_2O$ (152.2 mg, 0.89 mmol, 5.25 eq.) in deionized H_2O (0.8 mL). A yellow precipitate was immediately formed and isolated through vacuum filtration. The precipitate was washed with EtOH (3 x 10 mL) and dried *in vacuo* to yield APOSS$[CuCl_4]_4$ as a yellow powder (276.3 mg, 0.16 mmol, 95%).

Synthesis of (APOSS)$[CuCl_4]_4$ single crystals. To a vial containing 100 mg APOSSCl_8 (0.085 mmol) and 76.1 mg $CuCl_2{\cdot}2H_2O$ (0.447 mmol) was added 0.8 ml of deionized water. EtOH vapor was diffused into the solution over 2 days to yield yellow platelike crystals.

Intercalation of Tetracyanoethylene (TCNE) in (APOSS)$[CuCl_4]_4$. To a vial containing (APOSS)$[CuCl_4]_4$ (12.5 mg, 7.3 μmol) was added a solution of TCNE (37 mg, 73 μmol, 10 eq.) in THF (3 mL). The reaction was sonicated and heated at 50 °C for 1 week. The resulting yellow

powder was isolated through centrifugation and washed with THF (3 x 5 ml). Residual solvent was removed *in vacuo*.

Intercalation of Ferrocene (Fc) in (APOSS)[$CuCl_4$]$_4$. To a 4 mL vial was added (APOSS)[$CuCl_4$]$_4$ (10 mg, 5.8 μmol). To a 20 ml vial was added ferrocene (Fc) (10.8 mg, 58.4 μmol, 10 eq.) and the 4 mL vial containing (APOSS)[$CuCl_4$]$_4$ was placed inside. The 20 ml vial was sealed and heated at 75 °C for 1 week. The resulting powder was washed with isopropyl alcohol (3 x 5 ml) and dried *in vacuo*.

Synthesis of (APOSS)[$CuCl_{4-x}Br_x$]$_4$ from molecular precursors. To a vial containing ~ 10 mL of antisolvent (see table) was added a solution of $APOSSCl_8$, $APOSSBr_8$, $CuCl_2{\cdot}2H_2O$, and/or $CuBr_2$ in 0.5 mL deionized H_2O (see table). The resulting precipitate was isolated through vacuum filtration and washed with cold antisolvent (3 x 10 mL). The product was dried *in vacuo* to give the following yields: (APOSS)[$CuCl_{2.7}Br_{1.3}$]$_4$: 73.6 mg, 37.9 μmol, 89%, (APOSS)[$CuCl_{1.6}Br_{2.4}$]$_4$: 60.4 mg, 28.2 μmol, 92%, (APOSS)[$CuCl_{0.4}Br_{3.6}$]$_4$: 58.4 mg, 24.9 μmol, 76%, (APOSS)[$CuBr_4$]$_4$: 74.5 mg, 30.7 μmol, 94%.

Table S1. Mass of APOSS-halide and Cu-halide precursors used in the synthesis of (APOSS)[$CuCl_{4-x}Br_x$]$_4$. Values in parenthesis are reported in μmol.

X	$APOSSCl_8$	$APOSSBr_8$	$CuCl_2{\cdot}2H_2O$	$CuBr_2$	Antisolvent
1.3	50.0 mg (42.6)	-	19.0 mg (111.6)	24.9 mg (111.6)	EtOH
2.4	36.0 mg (30.7)	-	-	36.0 mg (161.2)	EtOH
3.6	-	50.0 mg (32.7)	14.6 mg (85.6)	19.1 mg (85.5)	IPA
4	-	50.0 mg (32.7)	-	36.5 mg (163.4)	IPA

Synthesis of (APOSS)[$CuCl_{4-x}Br_x$]$_4$ from APOSS[$CuCl_4$]$_4$. To vials containing 12.5 mg (7.3 μmol) of (APOSS)[$CuCl_4$]$_4$ and 2 mL CH_2Cl_2 was added a stock solution of 0.39 M Br_2 (0.78 M Br^-). Amount of stock solution added to each sample was incremented by 18.7 μL (14.6 μmol Br^- 2 eq.). Samples were allowed to react for 1 day, centrifuged, and then washed with CH_2Cl_2 (3 x 5 ml). The resulting powders were dried *in vacuo* and an average yield of 97% was obtained. Gas phase substitutions were performed by placing a 4 mL vial containing (APOSS)[$CuCl_4$]$_4$ inside a 20 mL vial containing excess Br_2. The 20 mL vial was sealed and let sit at room temperature for one week.

Synthesis of (APOSS)[$CuCl_{4-x}(SCN)_x$]$_4$. To vials containing 5.0 mg (2.9 μmol) (APOSS)[$CuCl_4$]$_4$ was added stoichiometric amounts of NH_4SCN dissolved in isopropyl alcohol. Reactions were sonicated for ~ 5 min before being heated at 60 °C overnight. The resulting powder was isolated through centrifugation and washed with isopropyl alcohol (3 x 5 ml). The powders were dried *in vacuo* and an average yield of 98% was obtained.

X-ray Photoelectron Spectroscopy. All XPS spectra were taken on a Kratos Axis-Ultra DLD spectrometer. This instrument has a monochromatized Al Kα X-ray and a low energy electron flood gun for charge neutralization. X-ray spot size for these acquisitions was on the order of 700 x 300 μm. Pressure in the analytical chamber during spectral acquisition was less than 5 x 10^{-9} Torr. Pass energy for survey and detailed spectra (composition) was 80 eV. Pass energy for the high-resolution spectra was 20 eV. The take-off angle (the angle between the sample normal and the input axis of

the energy analyzer) was 0° (0 degree take-off angle ~ 100 Å sampling depth). The Kratos Vision2 software program was used to determine peak areas and to calculate the elemental compositions from peak areas. CasaXPS was used to peak fit the high-resolution spectra. For the high-resolution spectra, a Shirley background was used and all binding energies were referenced to the C ls C-C bonds at 285.0 eV.

Scanning Electron Microscopy. SEM micrographs were collected on a Thermo Fisher Scientific Apreo-S with LoVac instrument. An accelerating voltage of 2 kV and beam current of 3 pA were employed. The instrument was made available by the University of Washington Molecular Analysis Facility. Samples were prepared by pressing loose powder between 2 Al studs.

Energy Dispersive X-ray Spectroscopy. EDX spectra and maps were collected on a Thermo Fisher Scientific Apreo-S with LoVac instrument located at the University of Washington Molecular Analysis Facility. Samples were prepared by pressing loose powder between 2 Al studs and measurements were performed with an accelerating voltage of 20 kV, beam current of 0.8 nA, and chamber pressure of 75-100 Pa. Small amounts of gaseous H_2O were introduced to the chamber to dissipate surface charge. For EDX mapping single crystalline samples of (APOSS)$[CuCl_4]_4$•χFc were mounted on carbon tape. The Aztec v4.4 software package was used to collect and analyze EDX spectra and maps. The signal from the Al stud was deconvoluted from the final elemental analysis. At% of each element was determined by taking the average of 3 different points on the same sample.

Gas Adsorption Measurements. Gas adsorption isotherms for pressures in the range 0-1 bar were measured by a volumetric method using a Micromeritics ASAP2020Plus. A typical sample of ~50 mg of perovskite was heated at 100 °C under 0.05 torr vacuum and transferred to a pre-weighed analysis tube, which was capped with a Micromeretics TranSeal and evacuated under dynamic vacuum at room temperature until an outgas rate of less than 3 μbar/min was achieved, typically 16 hours. For (APOSS)$[CuCl_4]_4$•χFc, a typical sample of ~50 mg of perovskite was heated at 80 °C under flowing N_2 gas and transferred to a pre-weighed analysis tube, which was capped with a Micromeretics TranSeal and evacuated under dynamic vacuum for 20 minutes at room temperature. The evacuated sample was transferred to an electronic balance and weighed again to determine the mass of sample. The tube was transferred back to the analysis port of the gas adsorption instrument. The outgas rate was again confirmed to be less than 3 μbar/min. For all isotherms, warm and cold free space corrections measurements were performed using ultra-high purity He gas (UHP grade 5.0, 99.999% purity). N_2 isotherms collected at 77 K were measured in liquid nitrogen baths. Oil-free vacuum pumps and oil-free pressure regulators were used for all measurements to prevent contamination of the samples during the evacuation process or of the feed gases during the isotherm measurements. BET surface areas were determined from N_2 adsorption data at 77 K using Micromeritics software. The parameters are listed below in Table S2.

Table S2. BET surface areas for porous perovskites.

Sample	(APOSS)$[CuCl_4]_4$	(APOSS)$[CuCl_4]_4$•1.04Fc	(APOSS)$[CuBr_4]_4$	(APOSS)$[CuCl_{3.46}(SCN)_{0.54}]_4$
SA_{BET} (m^2/g)	276	8.4	166	146
slope	0.353	11.2	0.586	0.666
y-int	3.48E–4	0.370	2.30E–4	4.3E–4
P_{low} (bar)	9.00E–7	1.09E–5	1.23E–7	1.43E–7
P_{high} (bar)	7.69E–5	.201	4.35E–5	7.61E–5
q_{sat} (mmol/g)	2.83	0.0863	1.70	1.50
C	1016	31	2550	1541

Thermal Gravimetric Analysis. Thermal gravimetric analysis (TGA) was performed using a TGAQ5000 (TA Instruments). A typical sample of ~2.5 mg of perovskite was heated to 600 °C with a heating rate of 10 °C/min in an N_2 flow of 25 mL/min.

(APOSS)$[CuCl_4]_4$ Single Crystal X-ray Diffraction. A yellow prism, measuring 0.11 x 0.10 x 0.10 mm^3 was mounted on a loop with oil. Data was collected at –73 °C on a Bruker APEX II single crystal X-ray diffractometer, Mo-radiation, equipped with a Miracol X-ray optical collimator.

Crystal-to-detector distance was 40 mm and exposure time was 30 seconds per frame for all sets. The scan width was 0.5°. Data collection was 97.4% complete to 25° in ϑ. A total of 3116 reflections were collected covering the indices, $-12 \le h \le 11$, $0 \le k \le 24$, $-9 \le l \le 40$. 1734 reflections were symmetry independent and the $R_{int} = 0.0302$ indicated that the data was excellent. Indexing and unit cell refinement indicated a face-centered orthorhombic lattice. The space group was found to be *F*mmm (No. 69).

The data appeared three-fold twinned (CELL_NOW)[4] and after multi-domain integration (SAINT, SADABS within the APEX2 software package by Bruker)[5] the data was merged utilizing twinabs.[6]

Solution by direct methods (SHELXT[7] or SIR97)[8] produced a complete heavy atom phasing model consistent with the proposed structure. The structure was completed by difference Fourier synthesis with SHELXL.[9] Scattering factors are from Waasmair and Kirfel.[10] Hydrogen atoms were placed in geometrically idealized positions and constrained to ride on their parent atoms with C---H distances in the range 0.95-1.00 Å. Isotropic thermal parameters U_{eq} were fixed such that they were $1.2U_{eq}$ of their parent atom U_{eq} for CH's and $1.5U_{eq}$ of their parent atom U_{eq} in case of methyl groups. All non-hydrogen atoms were refined anisotropically by full-matrix least-squares.

After multi-domain integration and scaling of the drilling, the structure solved well, but the silsesquioxane appeared disordered over two locations, and one of the chlorines (Cl3) was split as well. The contribution of some disordered solvent to the diffraction pattern (2 voids each 393$Å^3$ filled with 47 electrons in the unit cell) was analyzed and removed with SQUEEZE[11]

The structure is of high quality and ready for publication. **Table S2** summarizes the data collection details. **Figure S1** shows an ORTEP[12] of the asymmetric unit and the partially extended structure.

2. Supplementary Figures

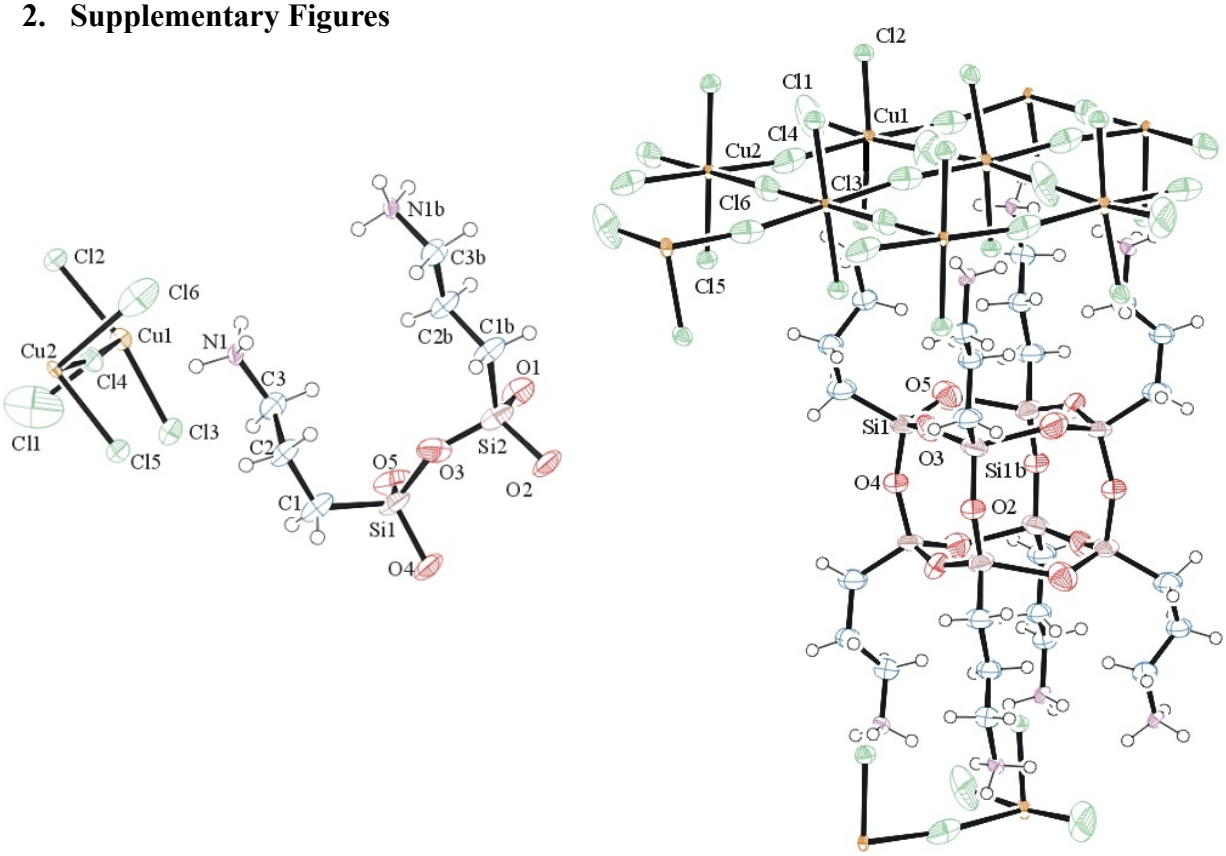

Figure S1. ORTEP of the asymmetric unit (left) and extended structure (right) with thermal ellipsoids at the 50% probability level. Disorder omitted for clarity.

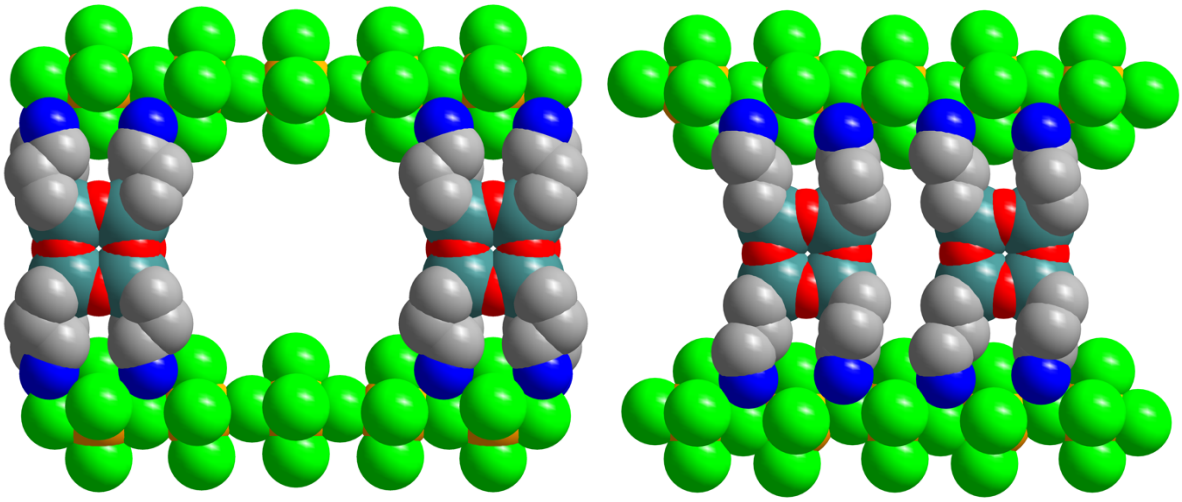

Figure S2. Space filling diagram of pores, with largest dimension, 17 Å (left), and shortest dimension, 6 Å (right), of each pore highlighted.

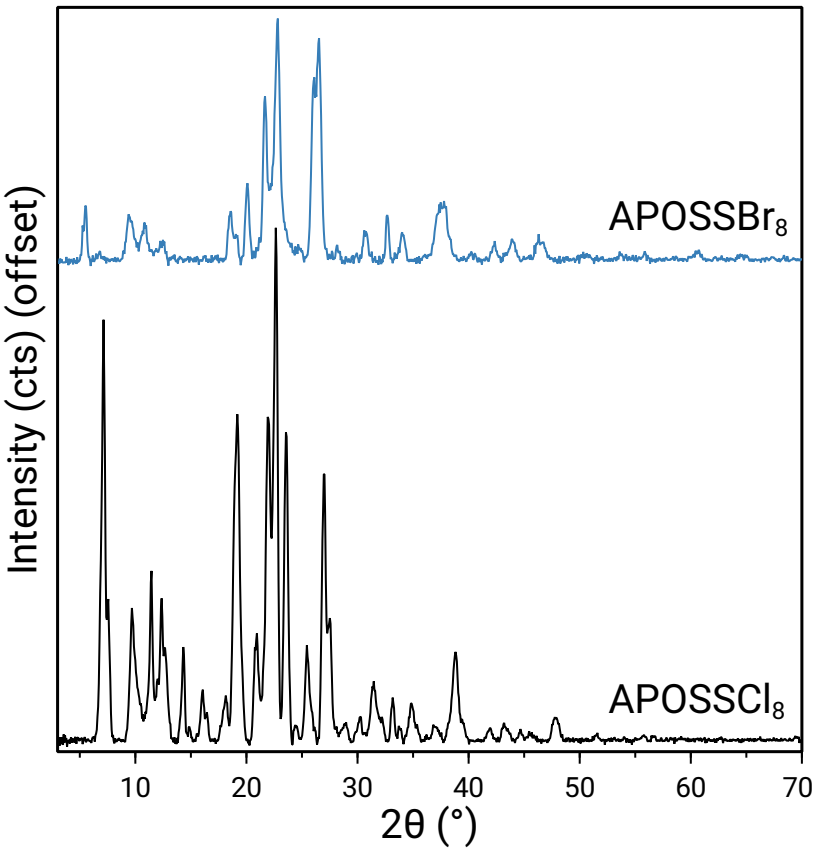

Figure S3. Powder X-ray diffraction pattern of $APOSSCl_8$ and $APOSSBr_8$

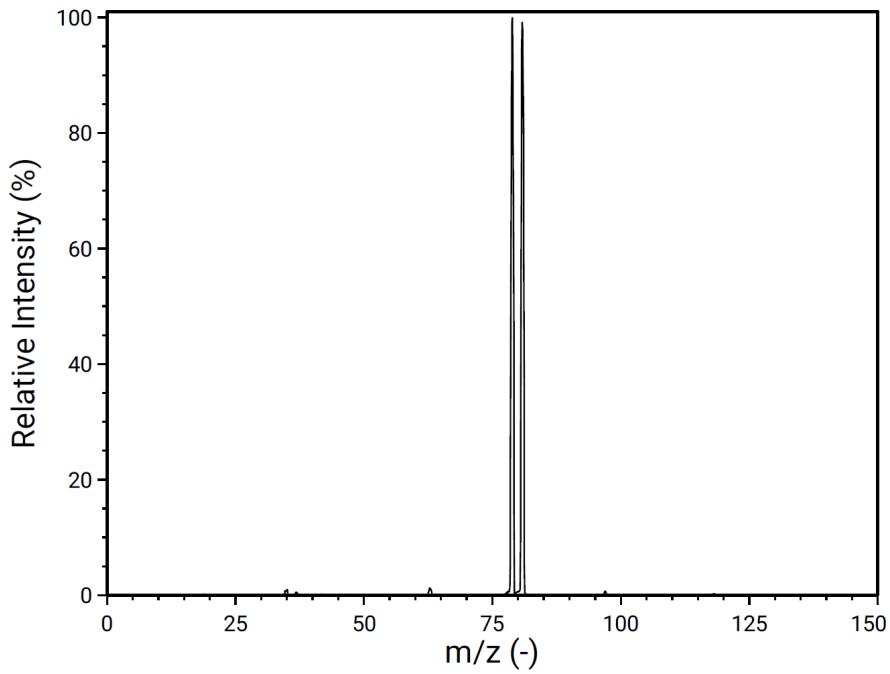

Figure S4. Negative ion mass spectrum of $APOSSBr_8$, showing full substitution of Cl^- for Br^-.

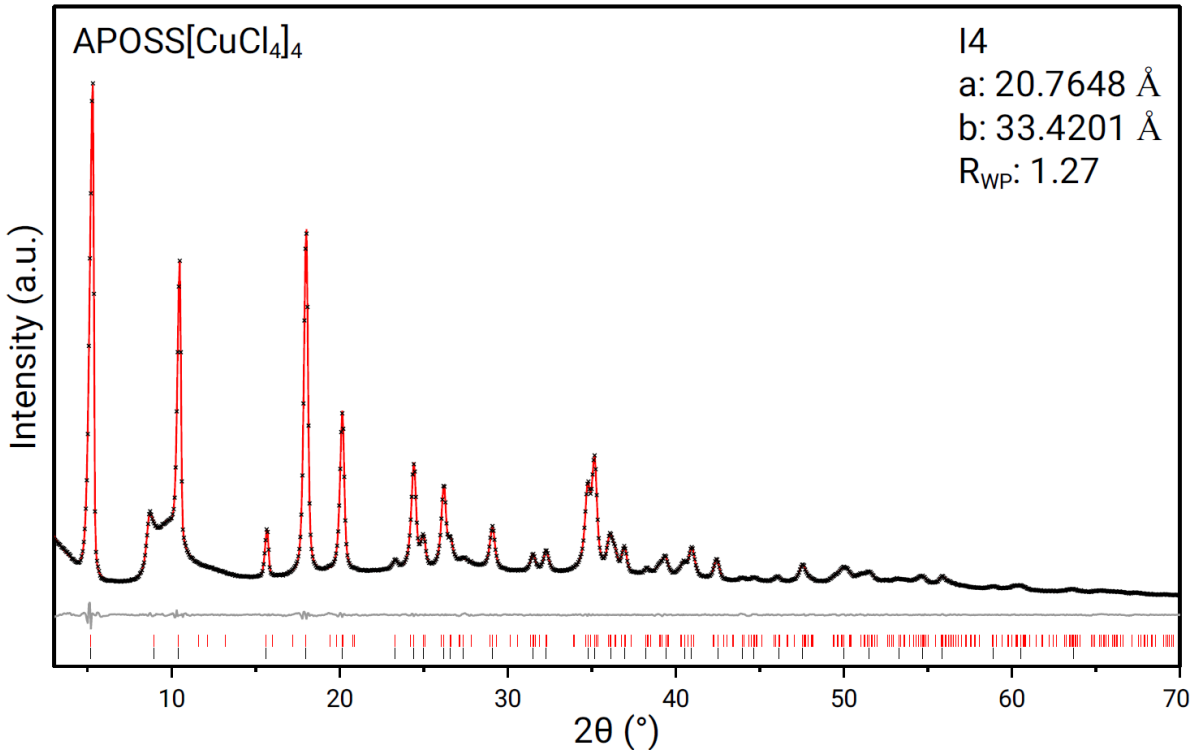

Figure S5. Pawley refinement of the PXRD data of (APOSS)[$CuCl_4$]$_4$, with experimental data in black crosses, the fit as a red line, and the residual as a gray line. Red hashes represent peaks predicted in the *I*4 space group and black hashes are peaks used in refinement of the structure.

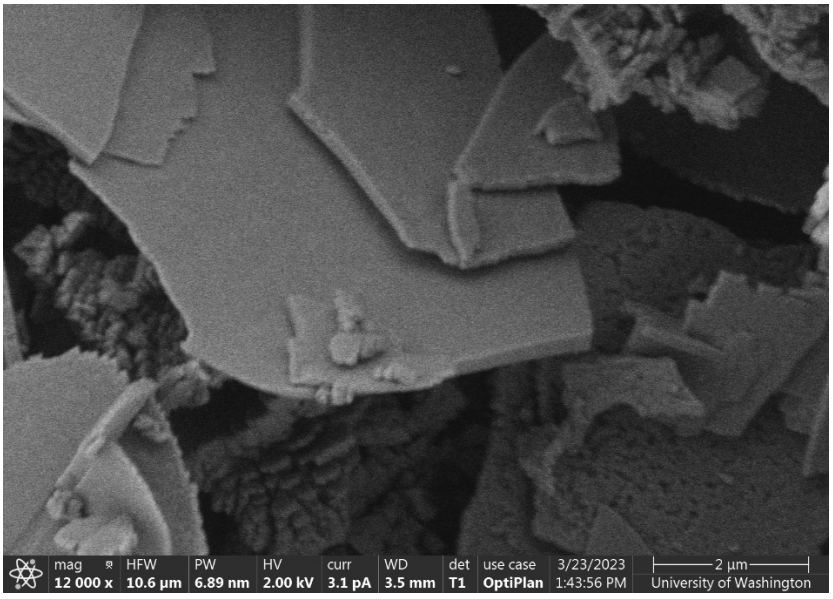

Figure S6. SEM micrograph of (APOSS)[$CuCl_4$]$_4$.

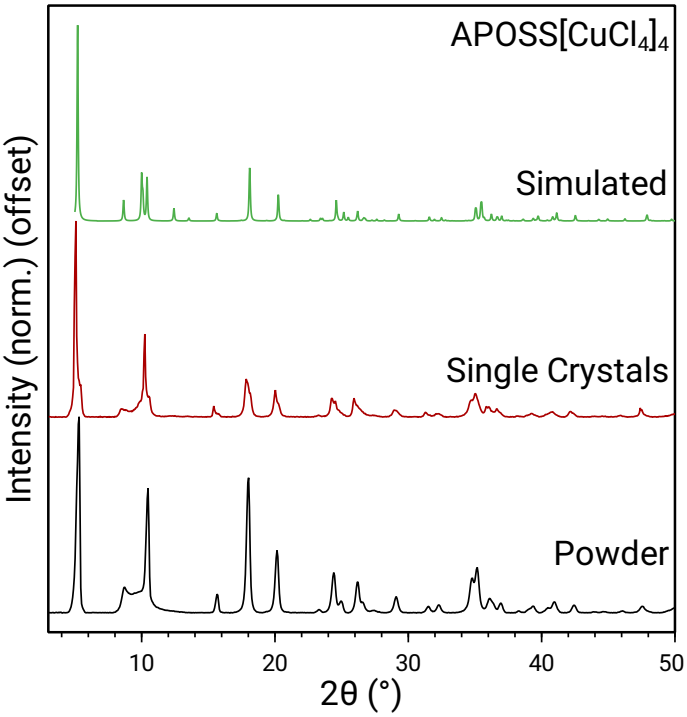

Figure S7. Comparison of PXRD patterns for (APOSS)[$CuCl_4$]$_4$: simulated data from SCXRD data, experimental data from finely ground single crystals, and experimental data from microcrystalline powder samples. Note that differences in the patterns are attributed to changes in temperature, where simulated data from SCXRD were collected at 100 K, while experimental data were collected at room temperature.

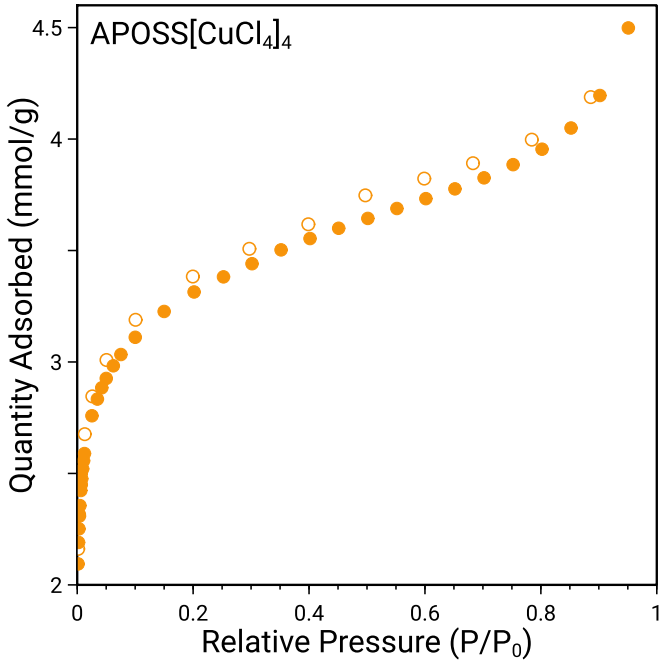

Figure S8. N_2 adsorption (filled) and desorption (empty) isotherm for (APOSS)[$CuCl_4$]$_4$. The BET surface area was calculated to be 276 m^2/g.

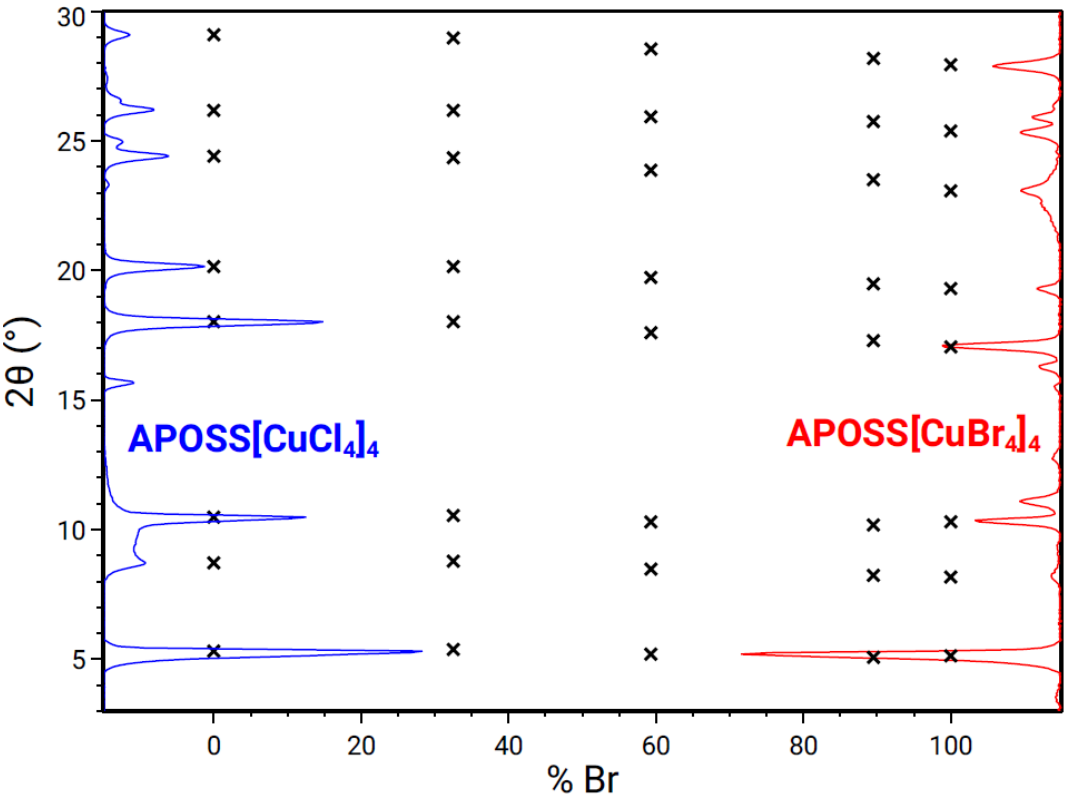

Figure S9. Peak shifts in (APOSS)[$CuCl_{4-x}Br_x$]$_4$ phases synthesized from mixed-halide precursors. Monotonic shifts to lower 2θ values indicate lattice expansion as Br^- (94 pm) replaces Cl^- (79 pm). The lack of shift in the 5.31° (002) and 10.48° (004) peaks indicate that the lattice is not expanding in the crystallographic c-axis.

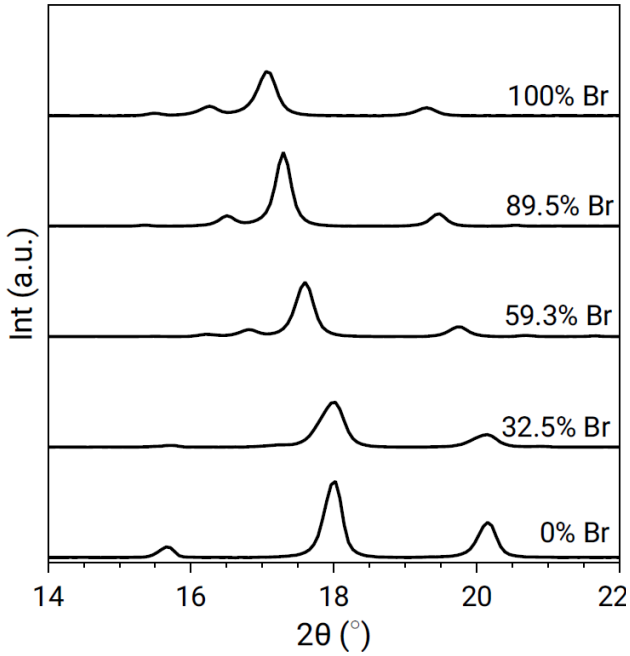

Figure S10. PXRD pattern for (APOSS)[$CuCl_{4-x}Br_x$]$_4$ phases synthesized from mixed-halide precursors showing the disappearance of the peak at 15.7° and the growth of the peak at 16.3°.

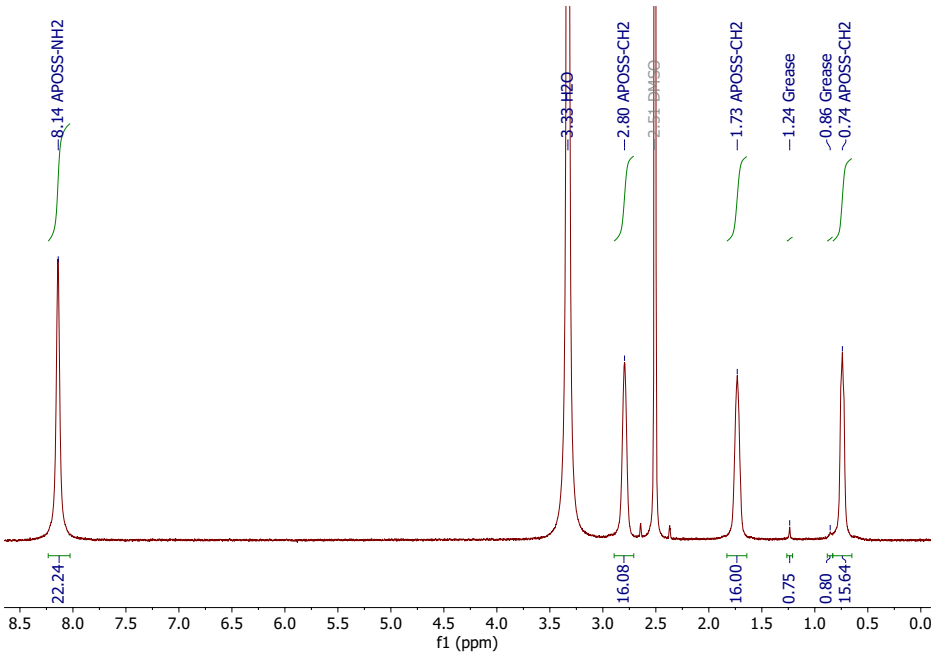

Figure S11. NMR spectrum of activated (APOSS)[$CuCl_4$]$_4$ in DMSO-d_6, showing absence of residual solvents.

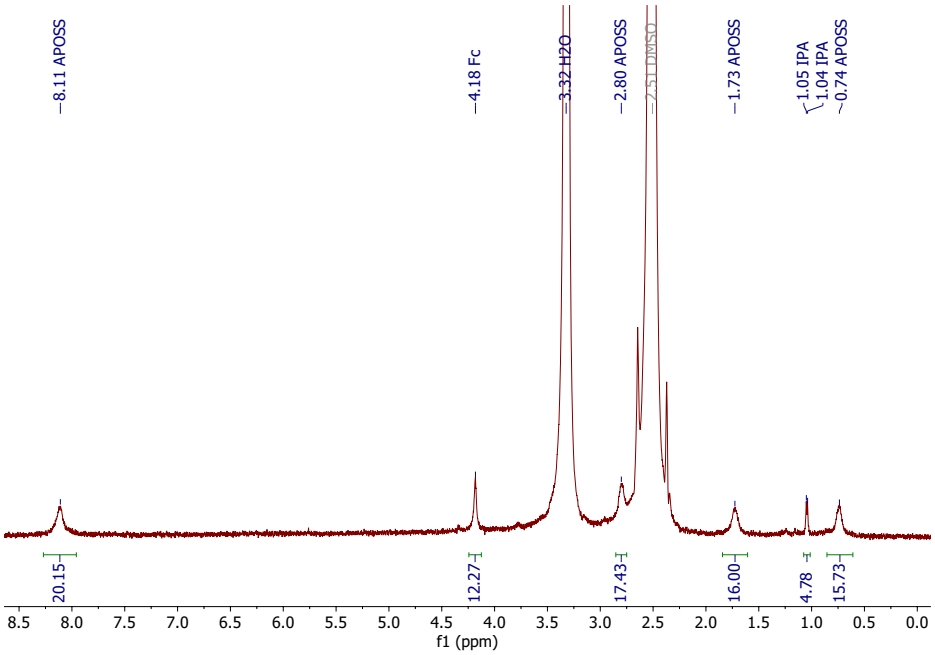

Figure S12. NMR spectrum of (APOSS)[$CuCl_4$]$_4$•1.22Fc. Ferrocene peak at 4.18 ppm is normalized to the $APOSSCl_8$ peak at 1.75 ppm after the material was dissolved in DMSO-d_6.

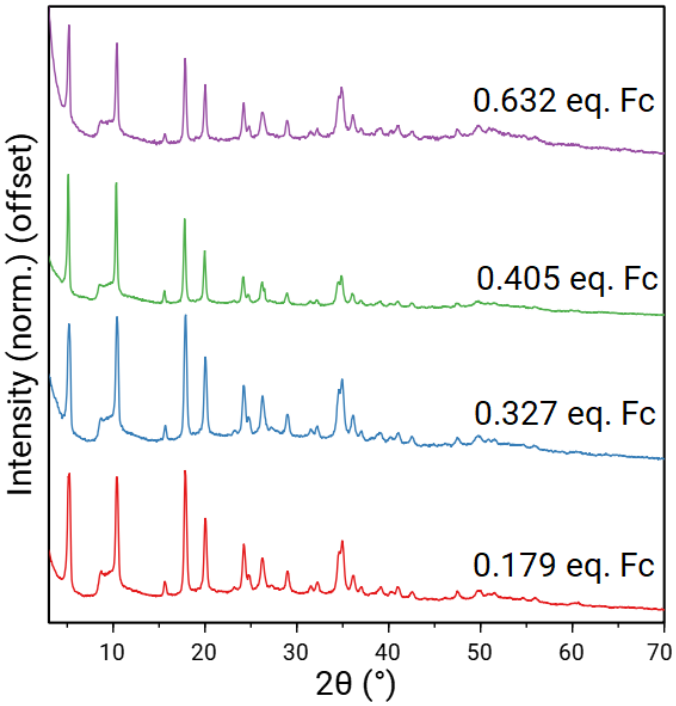

Figure S13. Powder X-ray diffraction of (APOSS)[$CuCl_4$]$_4$ at different exposure times to Fc gas: 1 day (red), 2 days (blue), 3 days (green), 4 days (purple). Fc content determined by NMR.

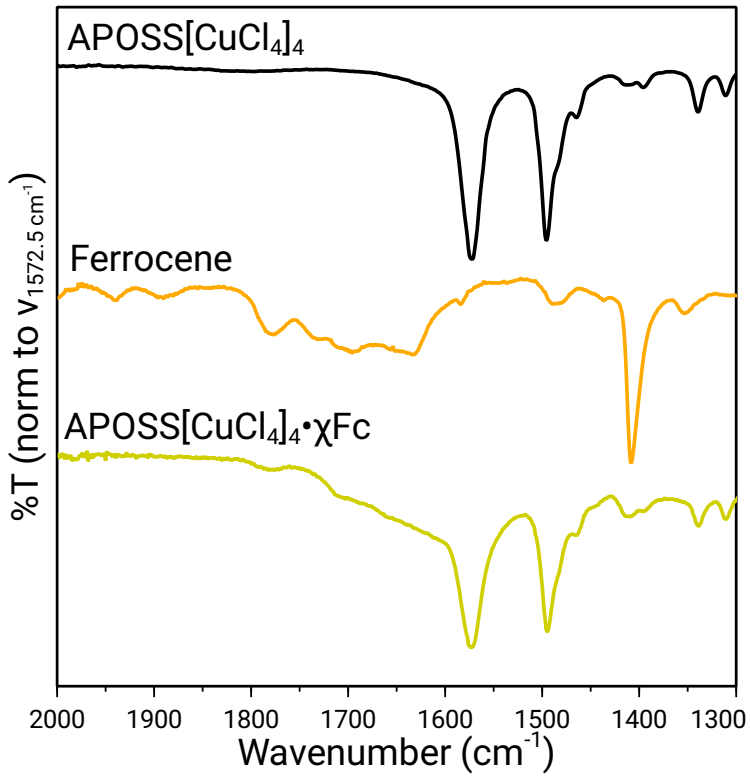

Figure S14. Infrared spectra of (APOSS)[$CuCl_4$]$_4$ (black), ferrocene (orange), and ferrocene-intercalated (APOSS)[$CuCl_4$]$_4$ (yellow).

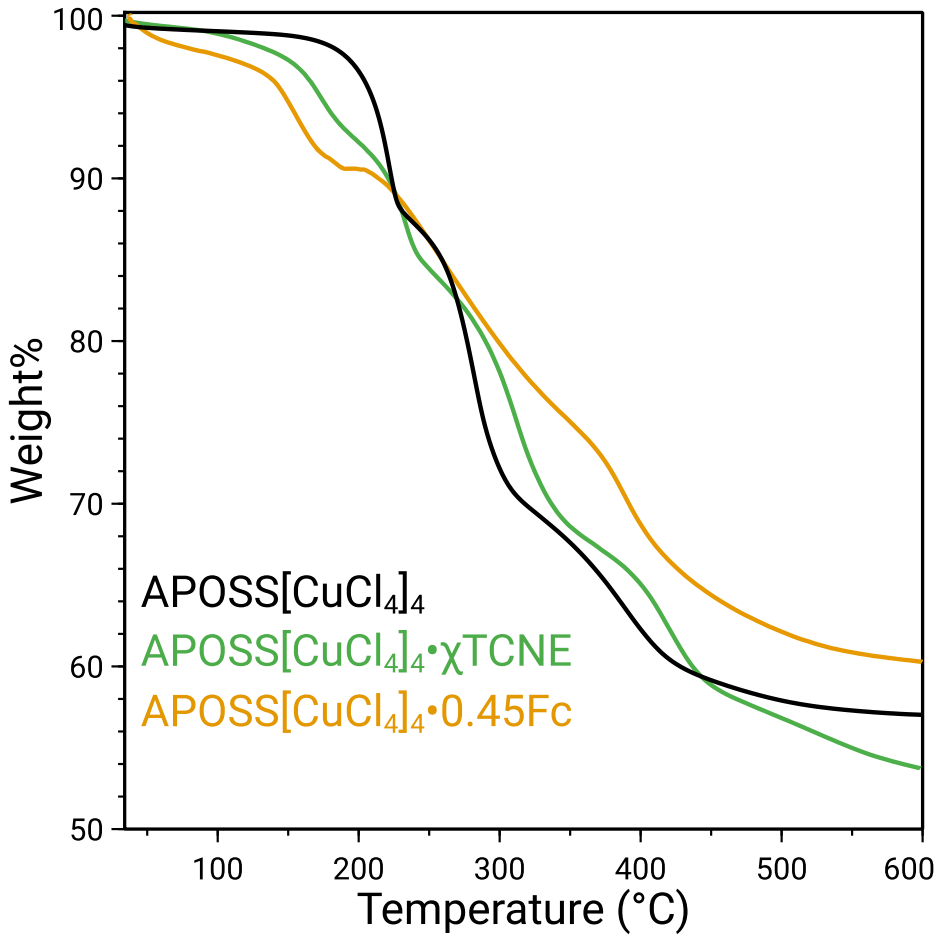

Figure S15. TGA plots for (APOSS)$[CuCl_4]_4$ (black), (APOSS)$[CuCl_4]_4$•χTCNE (green), and (APOSS)$[CuCl_4]_4$•0.45Fc (orange). Based on weight loss at 172 °C, χ in (APOSS)$[CuCl_4]_4$•χTCNE was calculated to be 0.83 which agrees with our previous attempts at quantifying TCNE content using FTIR spectroscopy.

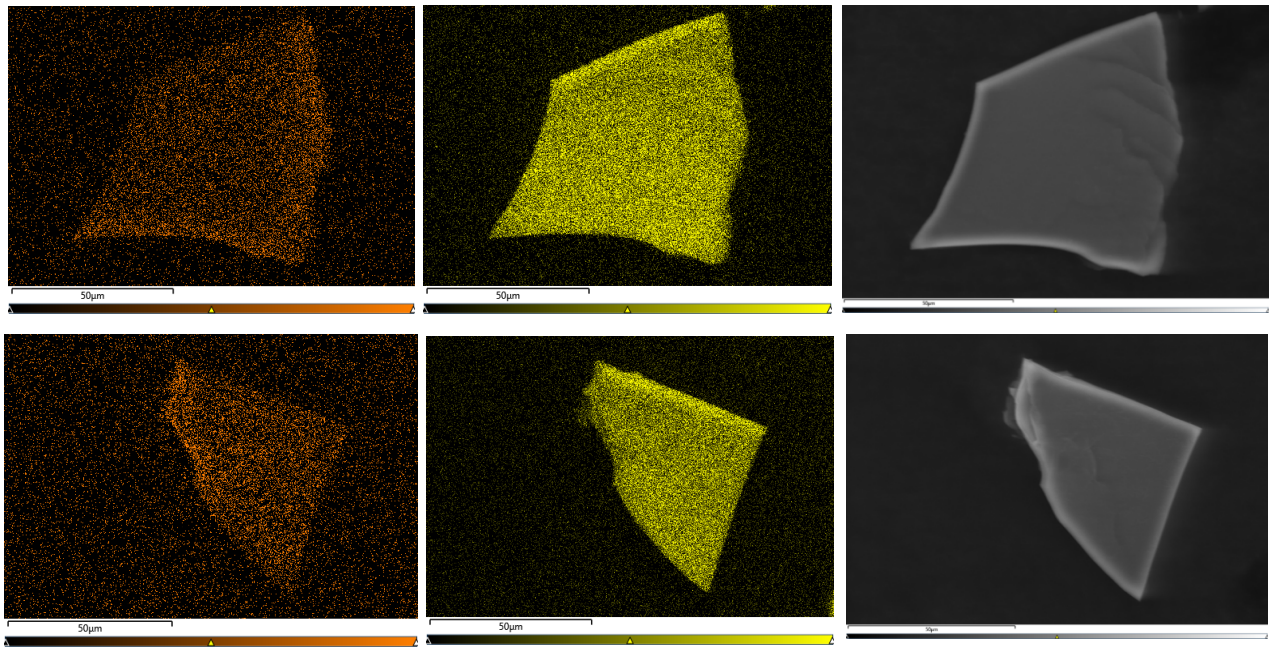

Figure S16. (left) Additional EDX maps of Fe distribution (orange dots) within flakes of (APOSS)$[CuCl_4]_4$. (center) EDX maps of Cu distribution (yellow dots) within flakes of (APOSS)$[CuCl_4]_4$. (Right) SEM micrographs of microcrystalline flakes of (APOSS)$[CuCl_4]_4$.

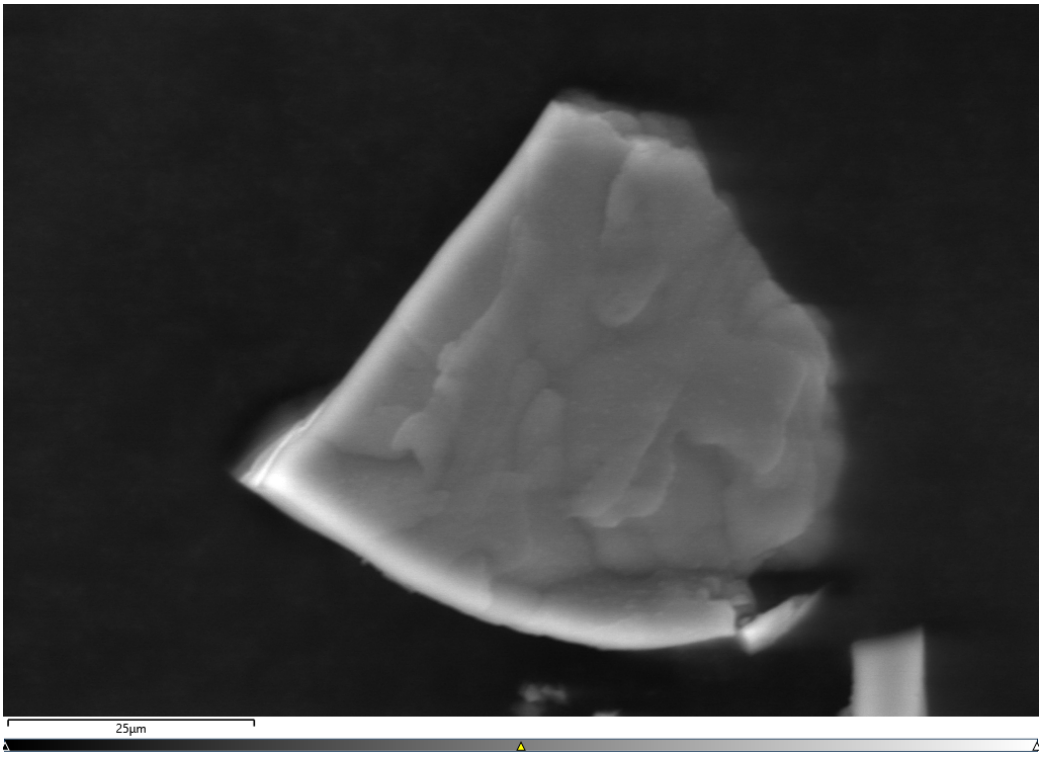

Figure S17. SEM micrograph of the microcrystalline flake of (APOSS)$[CuCl_4]_4$ mapped in the main text.

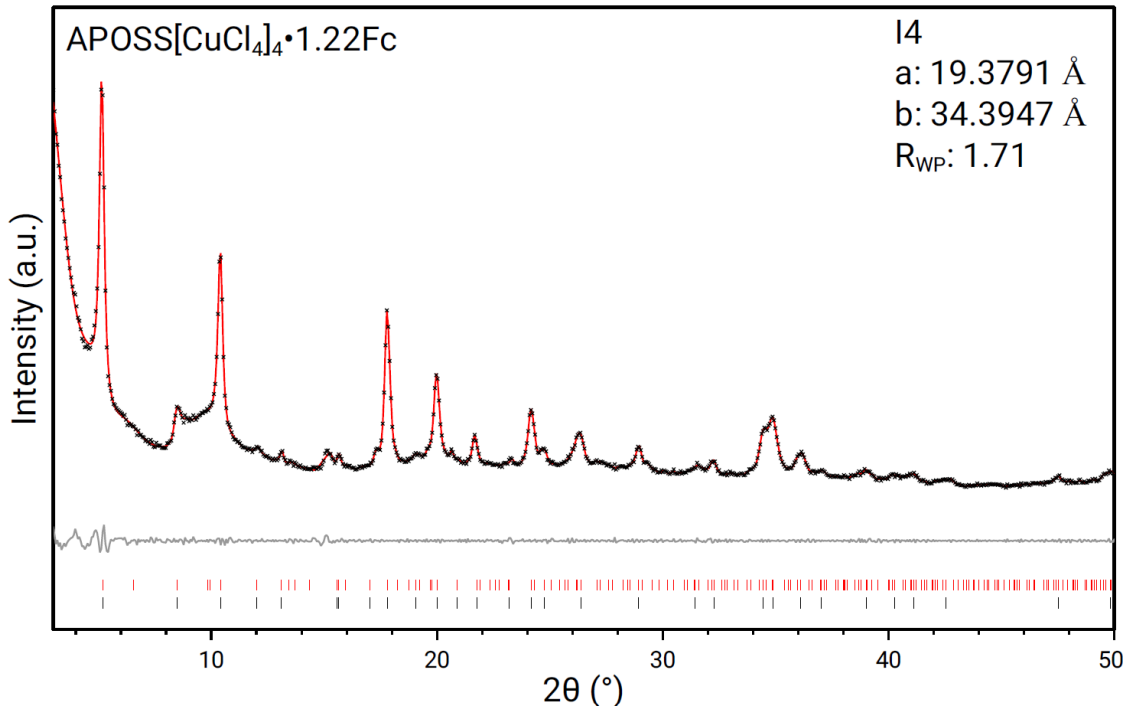

Figure S18. Pawley refinement of the PXRD data of (APOSS)[$CuCl_4$]$_4$•1.22Fc. Red hashes represent peaks predicted in the *I*4 space group and black hashes are peaks used in refinement of the structure.

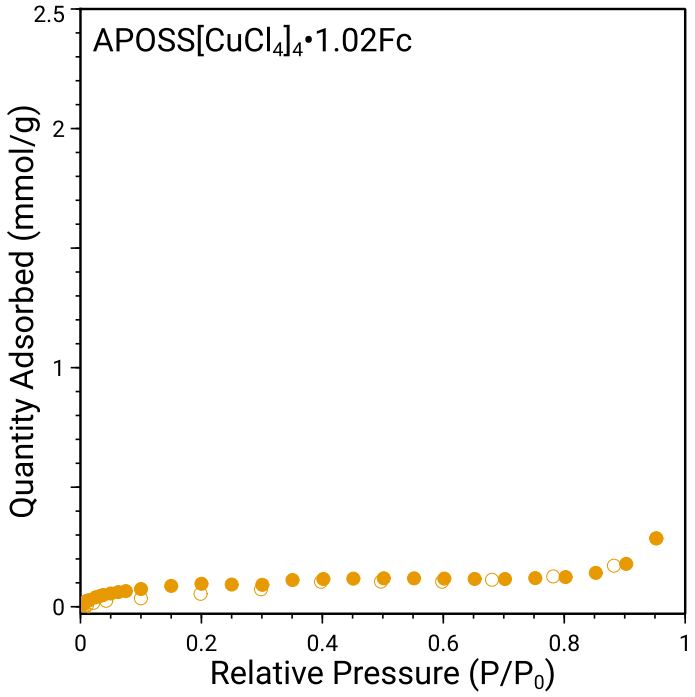

Figure S19. N_2 adsorption (filled) and desorption (empty) isotherms for APOSS[$CuCl_4$]$_4$•1.02Fc. The BET surface area was calculated as 8 m^2/g, indicating that intercalated Fc has taken up the pore space of the perovskite.

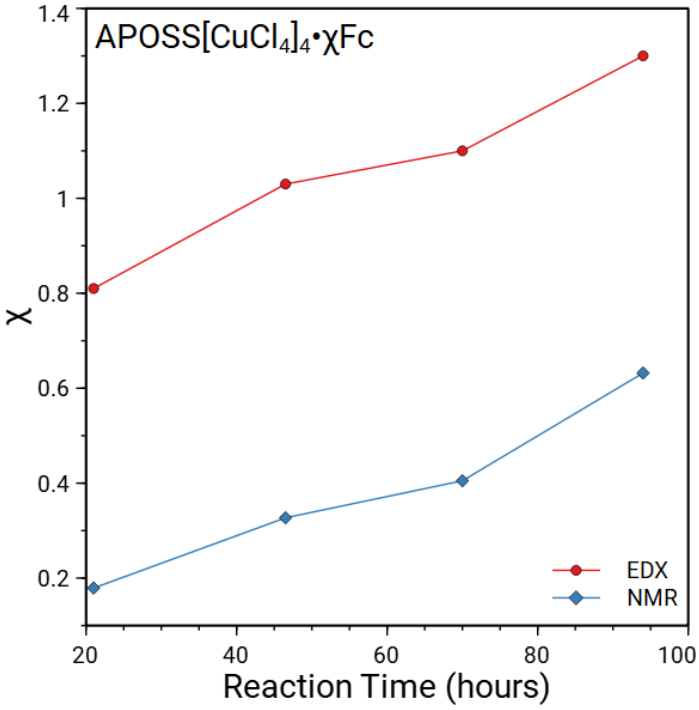

Figure S20. Comparison of Fc loading over different exposure times as determined by EDX (red circles) and NMR (blue diamonds).

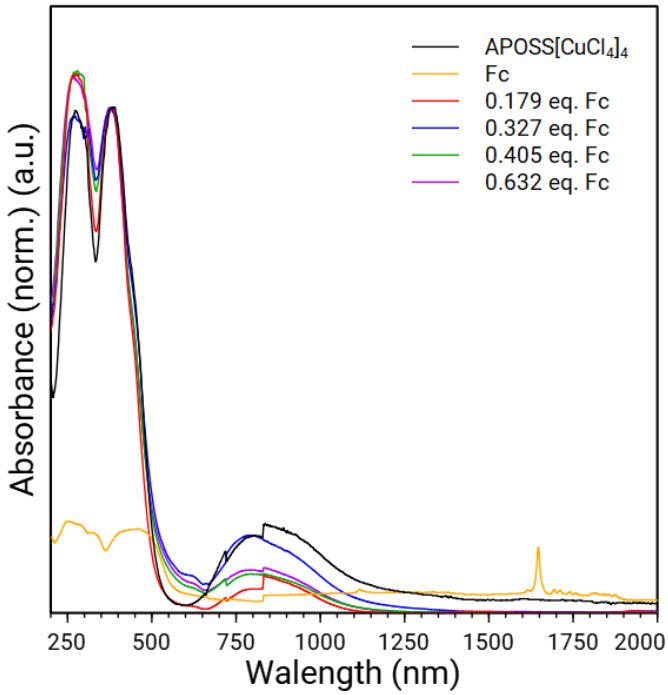

Figure S21. DRS Spectra of (APOSS)$[CuCl_4]_4$•χFc at various Fc loadings. Fc content determined by NMR.

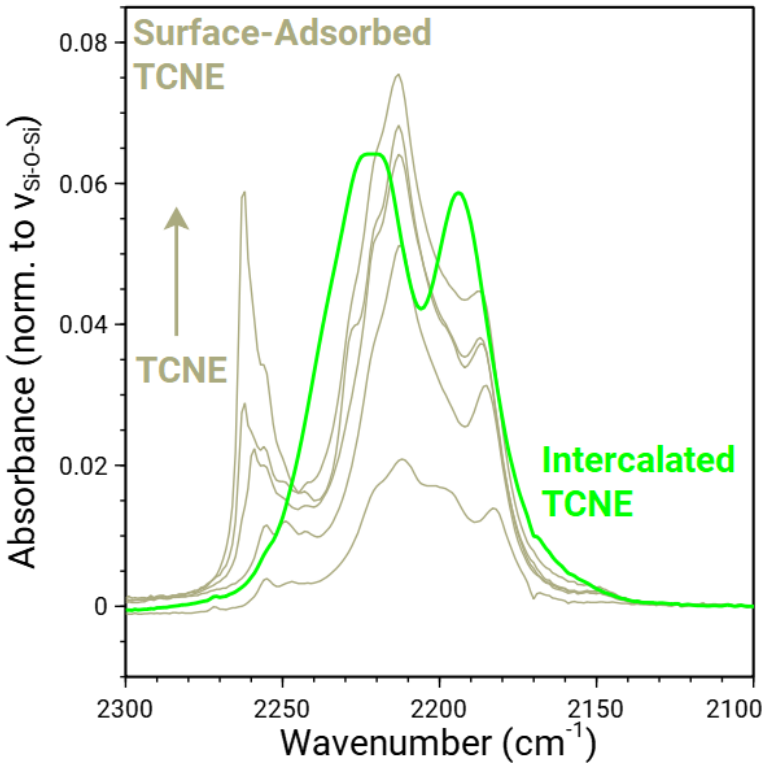

Figure S22. Comparison of nitrile stretching frequencies in intercalated TCNE and mechanical mixtures of (APOSS)$[CuCl_4]_4$ and TCNE, with mechanical prepared by mixing (APOSS)$[CuCl_4]_4$ with 1-5 equivalents of TCNE. All samples are measured in transmission mode as pressed pellets in a KBr matrix. The relative area of the normalized absorbance indicates that the TCNE intercalated of (APOSS)$[CuCl_4]_4$•*x*TCNE contains roughly 2-5 equivalents of TCNE per APOSS.

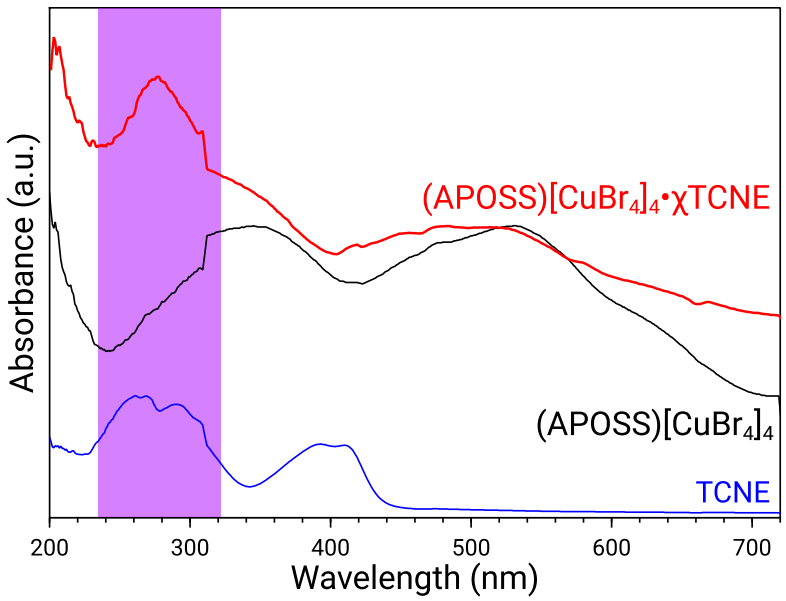

Figure S23. DRS spectrum of TCNE intercalated within (APOSS)$[CuBr_4]_4$, with features corresponding to TCNE highlighted.

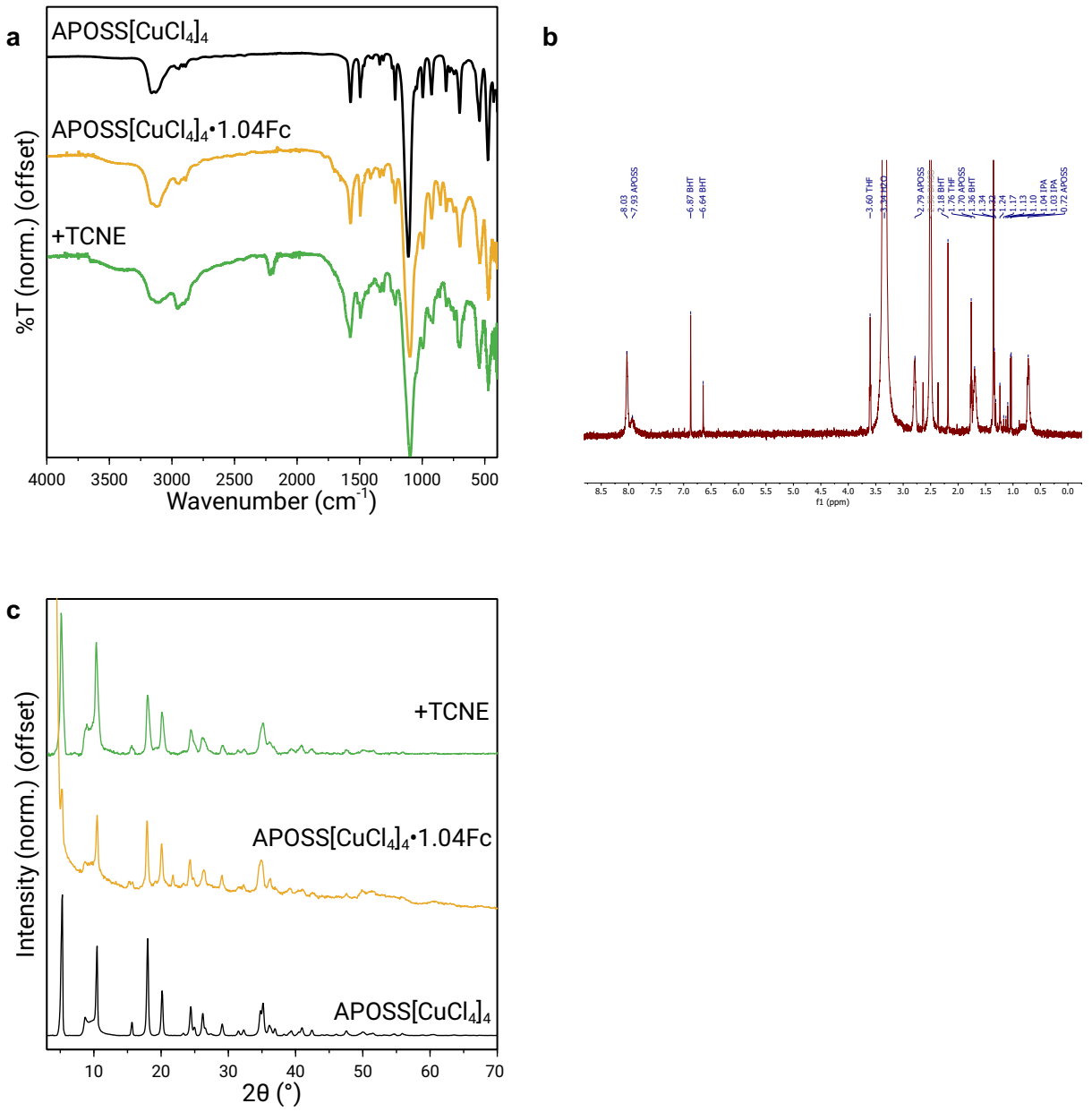

Figure S24. Data collected after exposing (APOSS)$[CuCl_4]_4$•1.04Fc to a solution of TCNE in THF to show replacement of Fc with TCNE. The IR data (**a**) shows the growth of TCNE-based stretches at approximately 2200 cm^{-1}, ^1H NMR spectra in DMSO-d_6 (**b**) shows a clear absence of Fc which is expected at 4.18 ppm (all extra peaks are attributed to residual solvent, solvent stabilizers, or vacuum grease), and PXRD patterns (**c**) shows that the perovskite structure is retained.

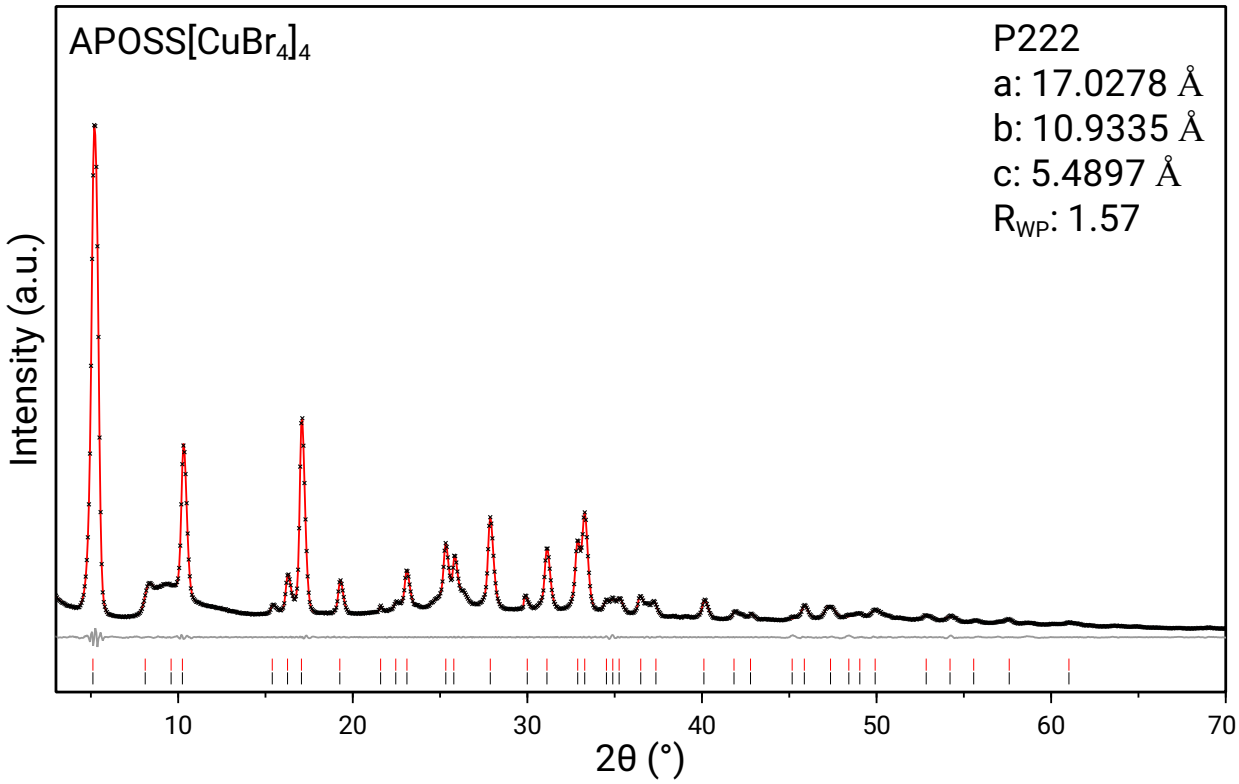

Figure S25. Pawley refinement of the PXRD data of (APOSS)[$CuBr_4$]$_4$. Red hashes represent peaks predicted in the *P*222 space group and black hashes are peaks used in refinement of the structure.

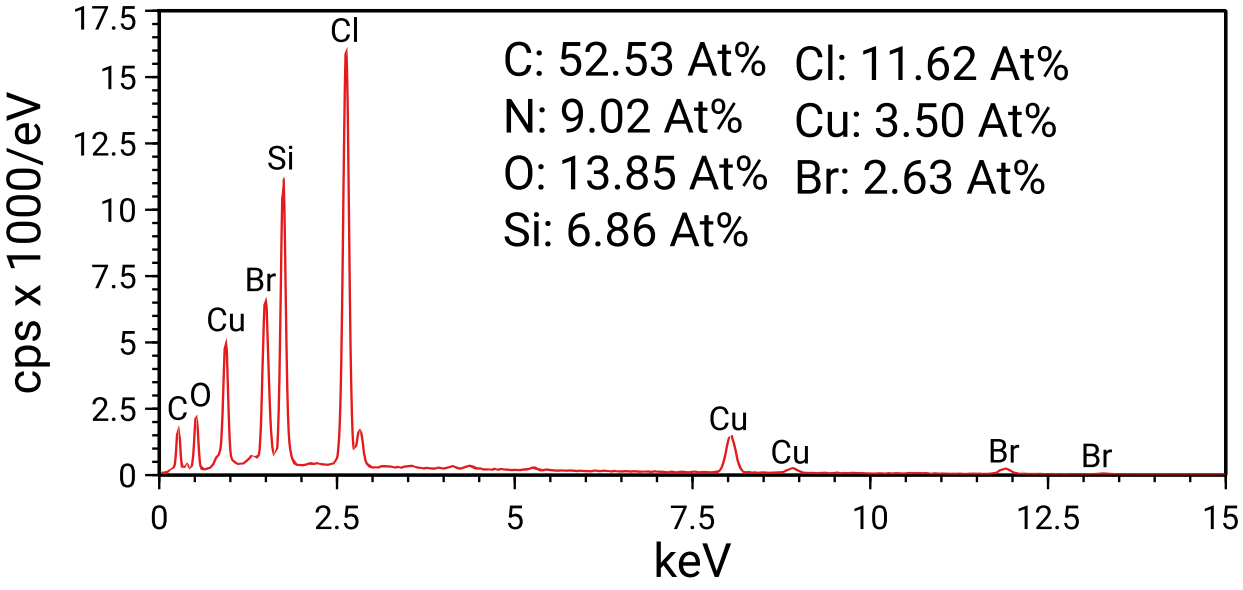

Figure S26. EDX spectrum of gas-phase Br^- substitution in (APOSS)[$CuCl_4$]$_4$. %Br calculated by dividing At% Br by the sum of At% Br and At% Cl.

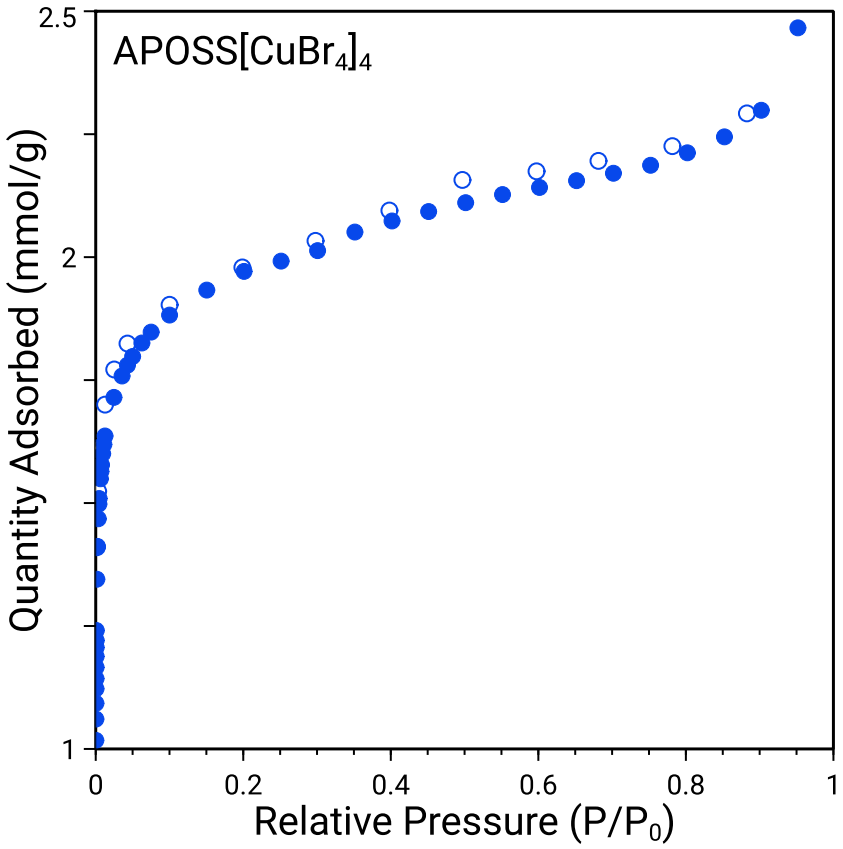

Figure S27. N_2 adsorption (filled) and desorption (empty) isotherms for (APOSS)[$CuBr_4$]$_4$. BET surface area was calculated to be 166 m^2/g.

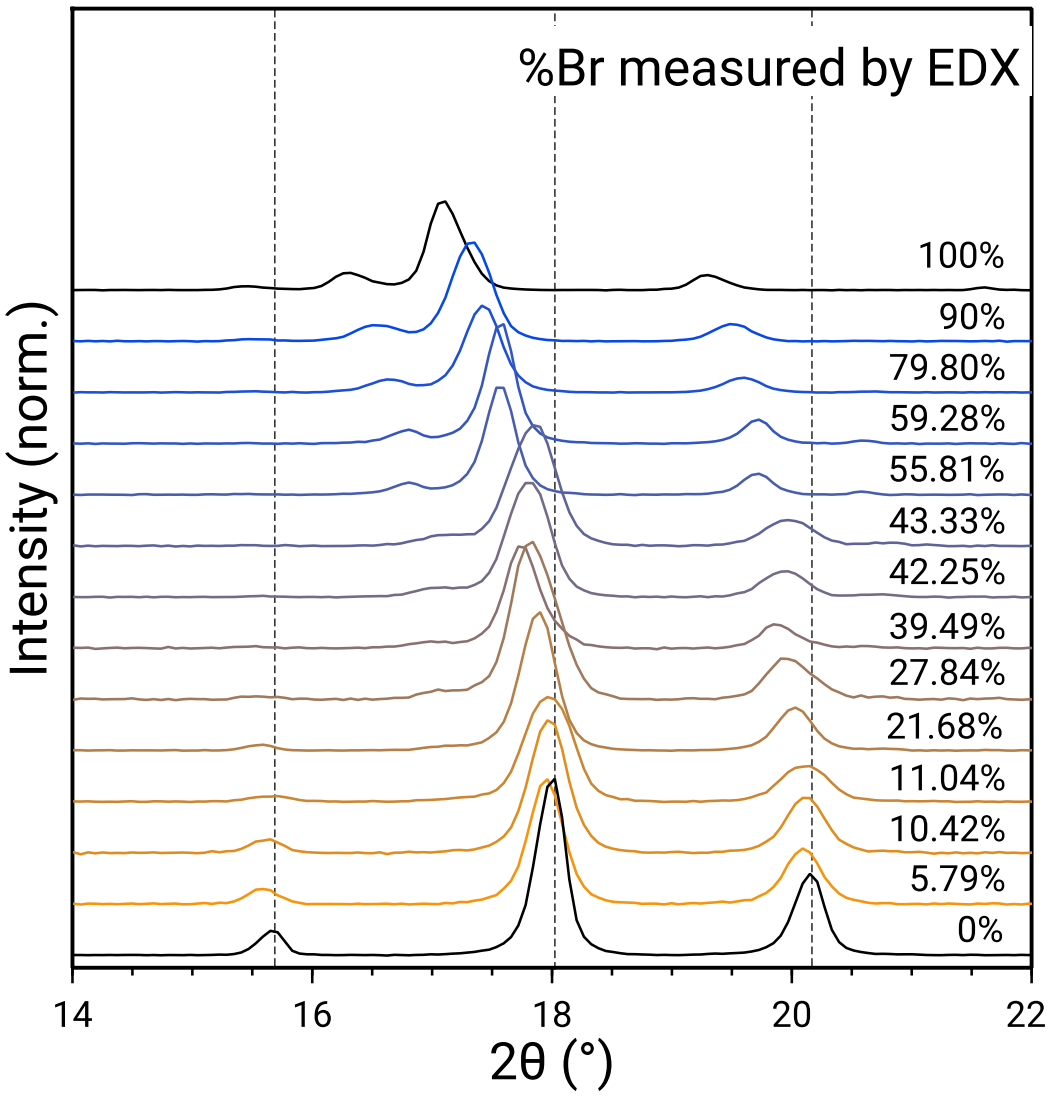

Figure S28. PXRD pattern for (APOSS)[$CuCl_{4-x}Br_x$]$_4$ phases from post-synthetic halide substitution showing the disappearance of the 15.7° peak and the growth of the 16.3° peak.

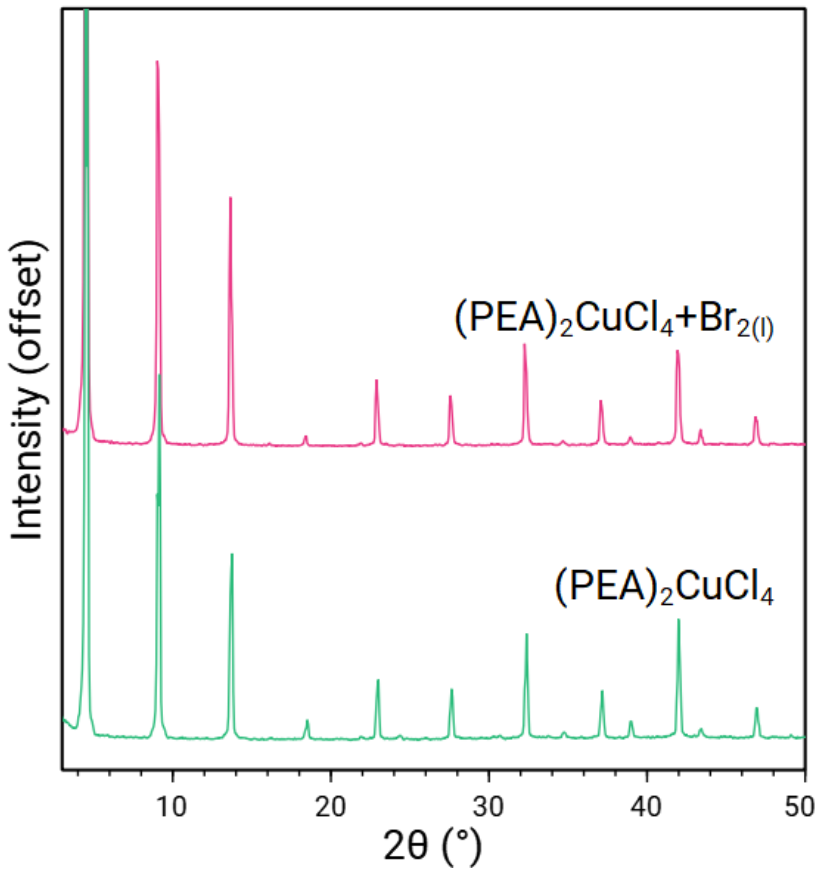

Figure S29. Powder X-ray diffraction pattern of $(PEA)_2[CuCl_4]$ control exposed to Br_2 stock solution in CH_2Cl_2.

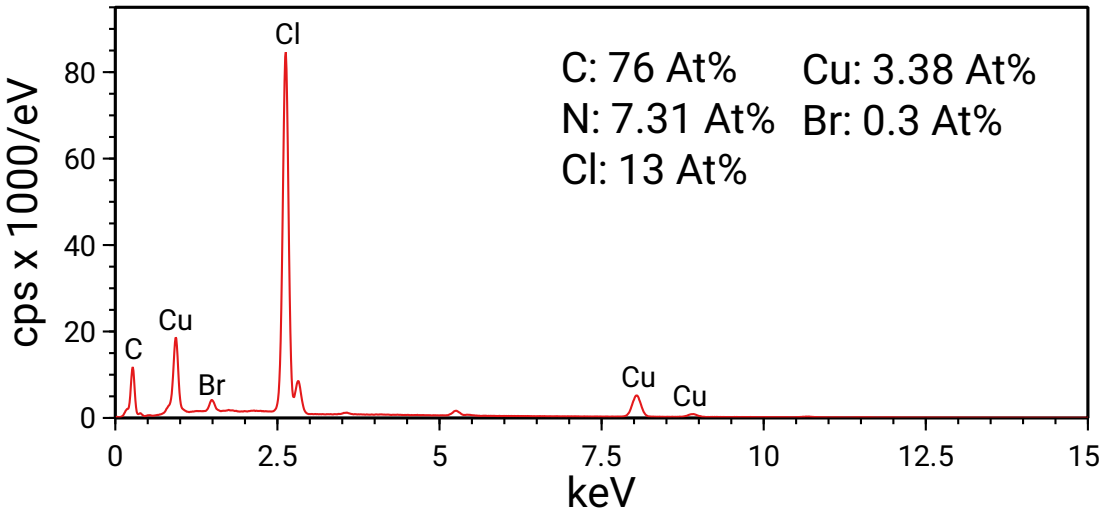

Figure S30. EDX spectrum of liquid phase Br^- substitution in $(PEA)_2CuCl_4$. %Br calculated by dividing At% Br by the sum of At% Br and At% Cl.

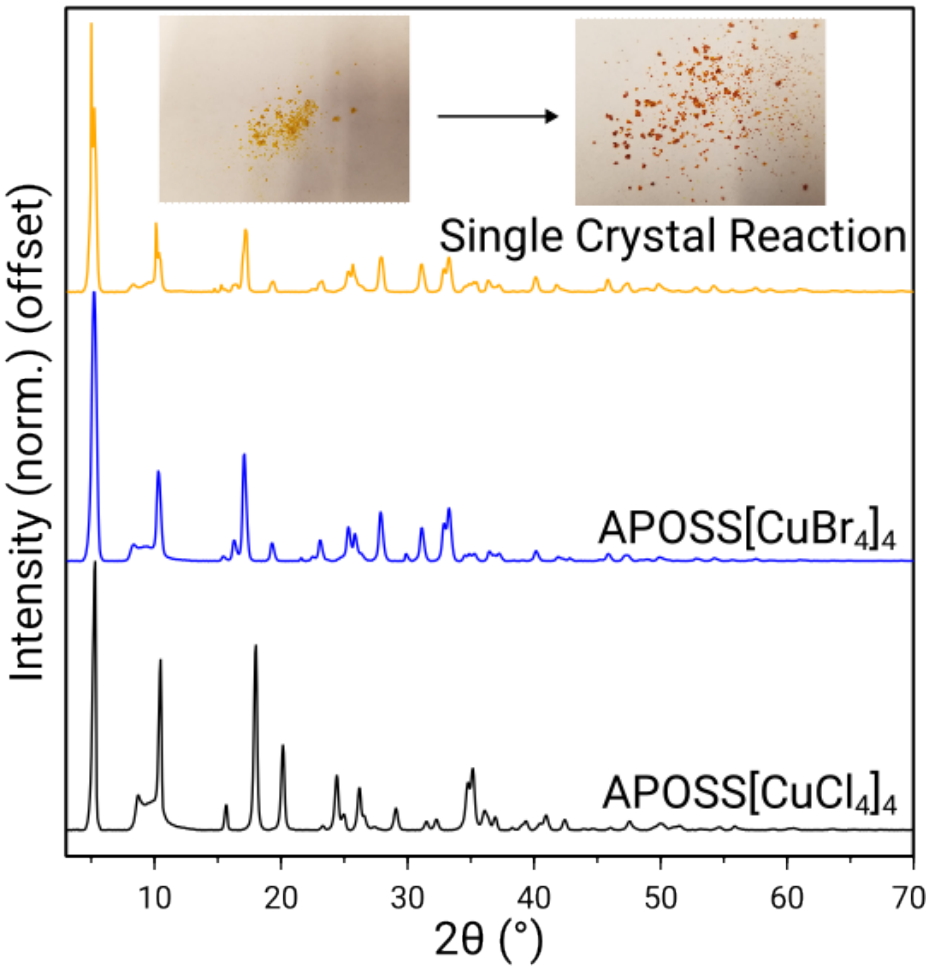

Figure S31. Powder X-ray diffraction pattern of (APOSS)$[CuCl_4]_4$ single crystals before and after exposure to Br_2 stock solution in CH_2Cl_2.

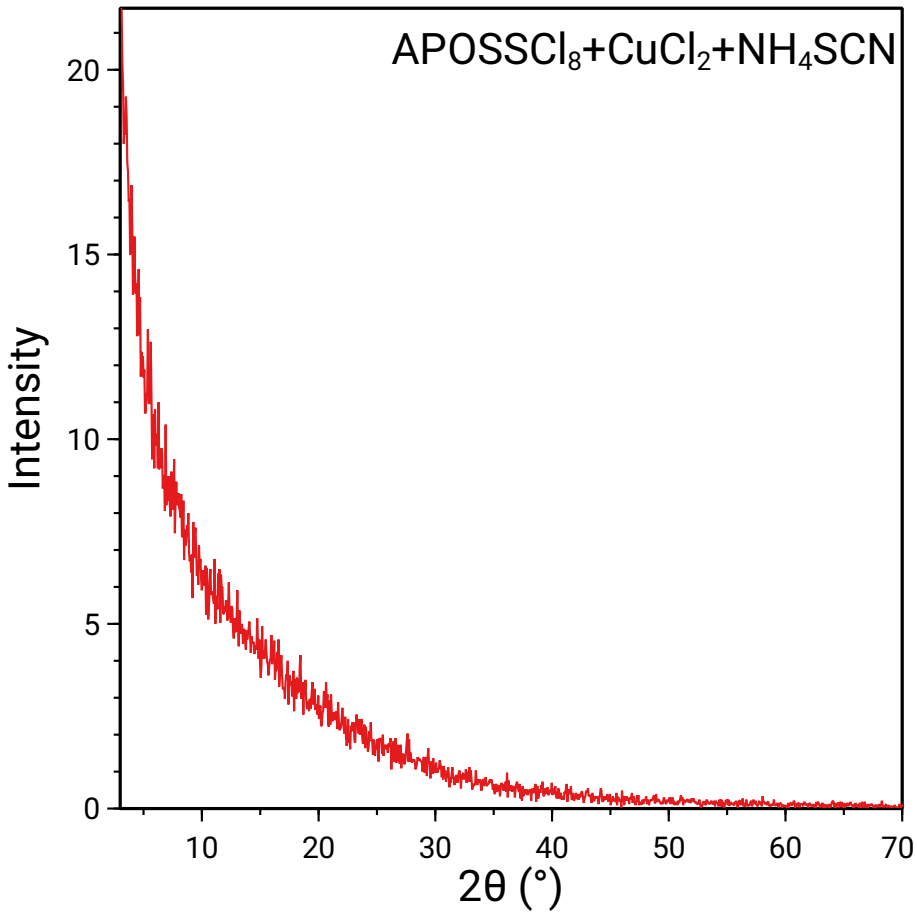

Figure S32. Representative control experiment of solution-phase reaction of APOSS-Cl_8, $CuCl_2$, and NH_4SCN, generating a colorless amorphous product. The thiocyante perovskites shown in the main text are generated much easier through post-synthetic modification.

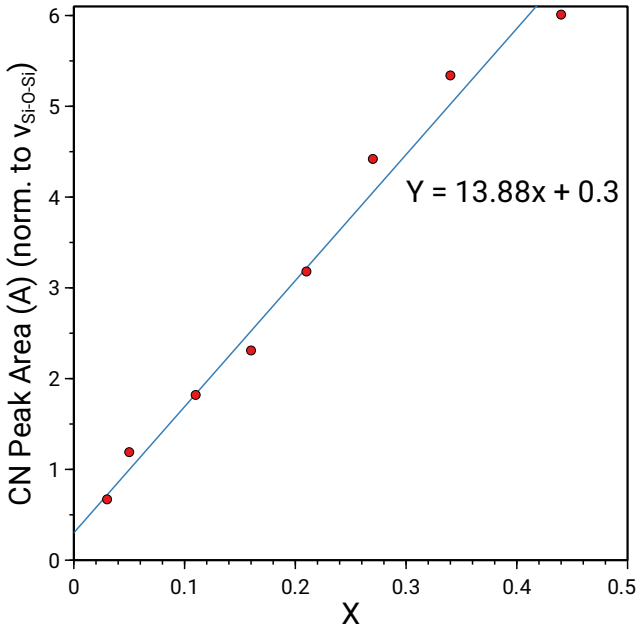

Figure S33. Comparison of integrated area of thiocyanate IR stretch at 2087 cm^{-1} and sulfur content in (APOSS)[$CuCl_{4-x}(SCN)_x$]$_4$ as determined by EDX.

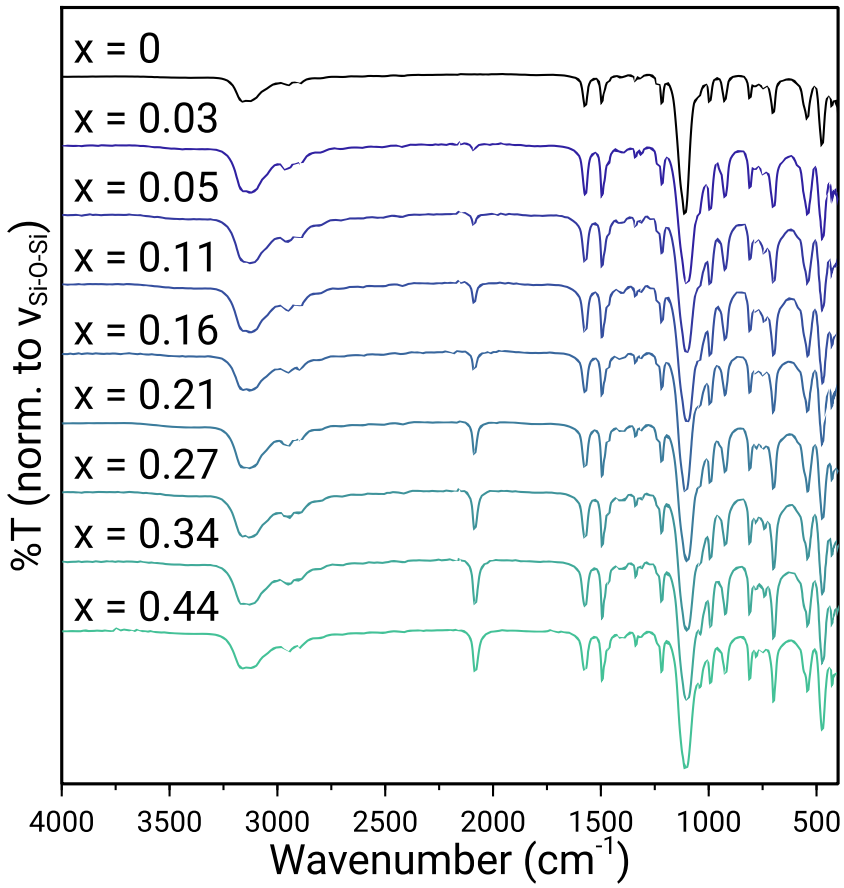

Figure S34. Full FTIR spectra of (APOSS)[$CuCl_{4-x}(SCN)_x$]$_4$ at $0 \leq x \leq 0.44$.

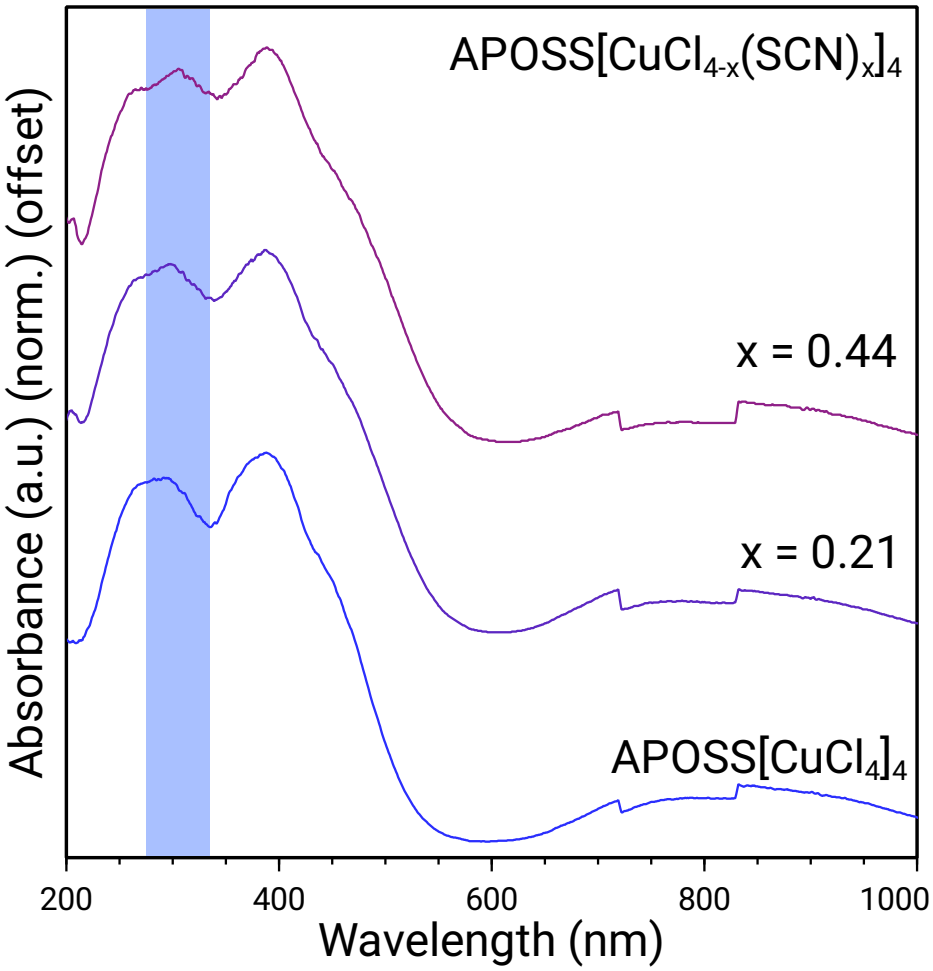

Figure S35. DRS spectra of (APOSS)[$CuCl_{4-x}(SCN)_x]_4$ at $0 \leq x \leq 0.44$, with new LMCT transition from Cu-SCN bond highlighted.

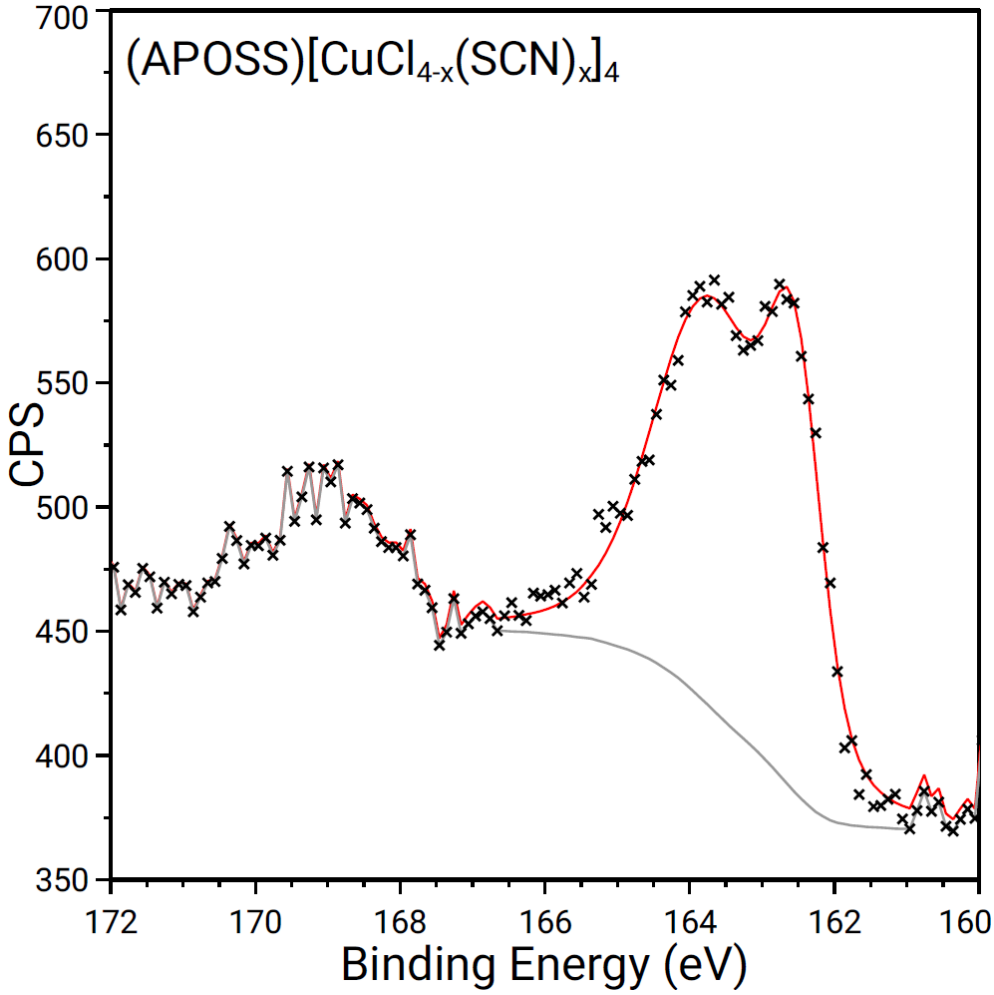

Figure S36. Full XPS S 2p spectrum of (APOSS)[$CuCl_{4-x}(SCN)_x]_4$. Broad peak at 169 eV is attributed to free NH_4SCN.[13]

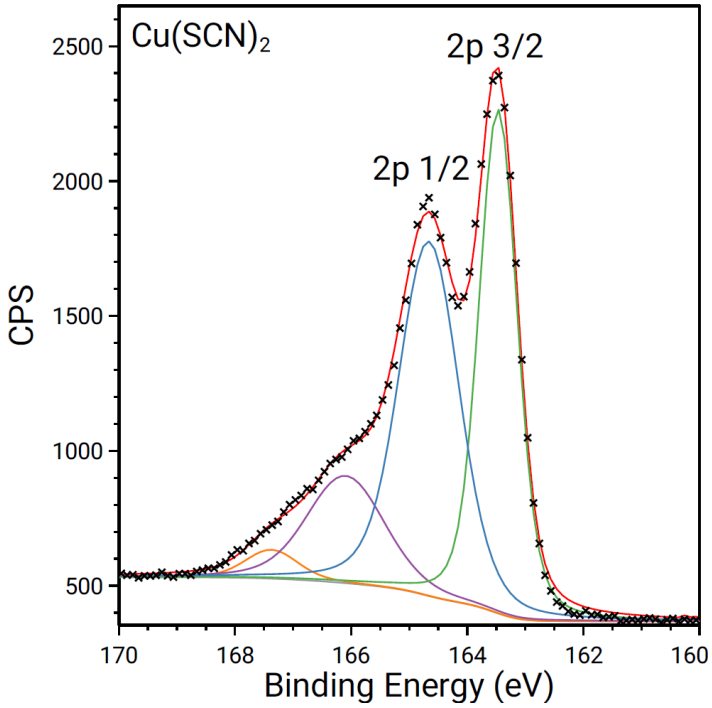

Figure S37. High resolution XPS spectrum of the S 2p region of $Cu(SCN)_2$.

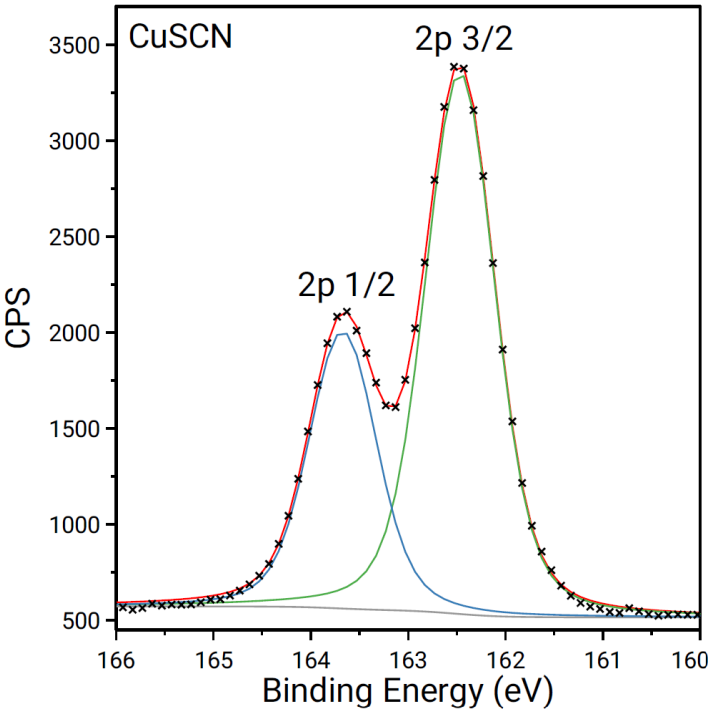

Figure S38. High resolution XPS spectrum of the S 2p region of Cu(SCN).

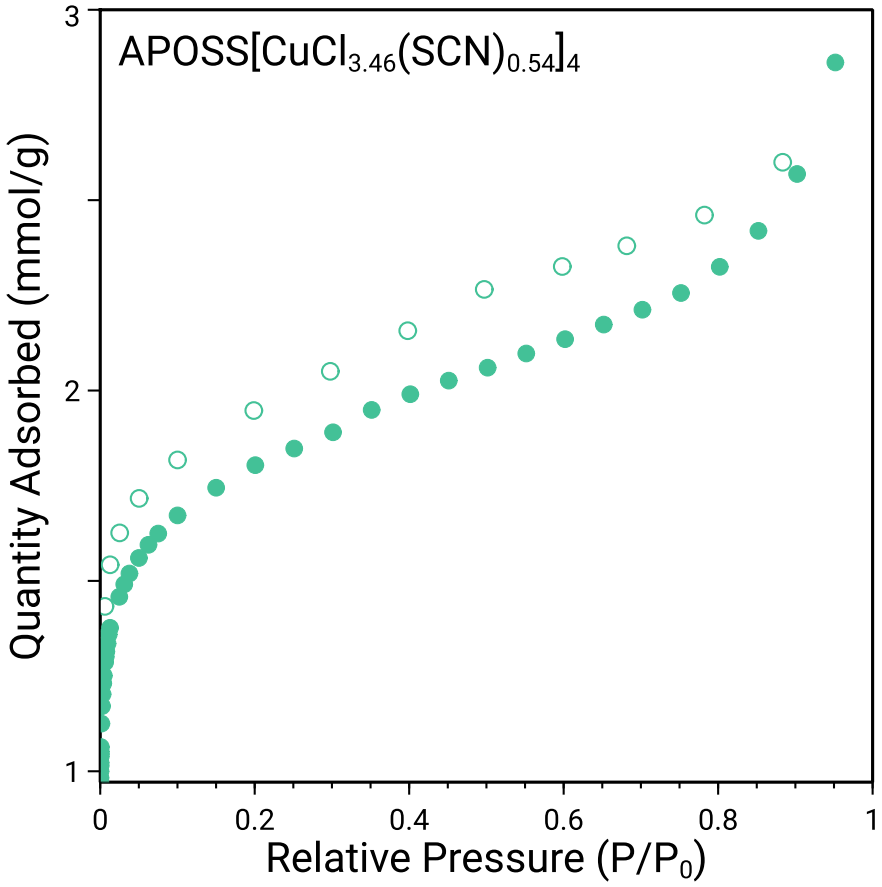

Figure S39. N_2 adsorption (filled) and desorption (empty) isotherms for (APOSS)[$CuCl_{3.46}(SCN)_{0.54}$]$_4$. The BET surface area was calculated to be 146 m^2/g.

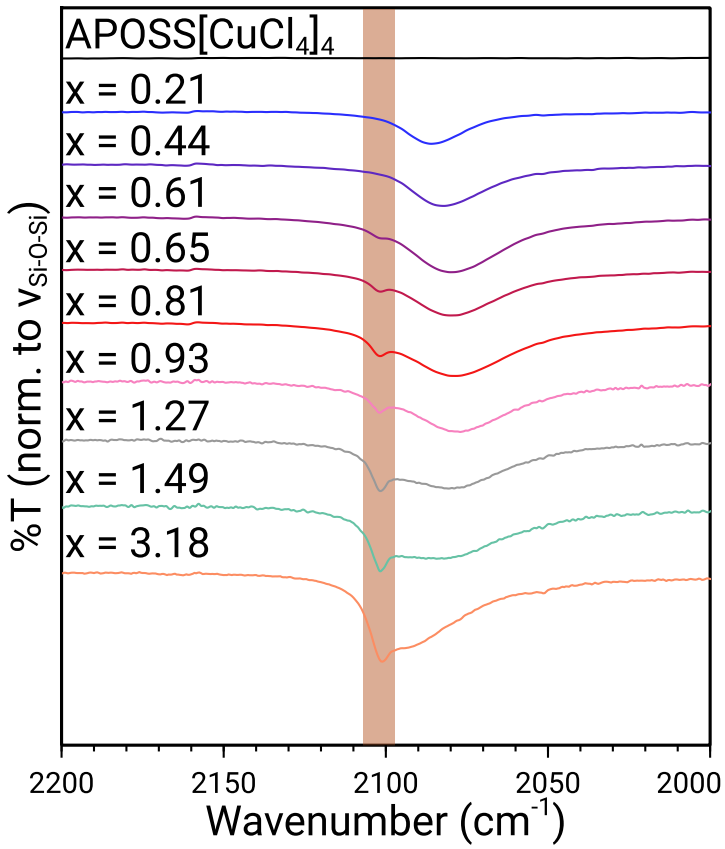

Figure S40. FTIR spectra of the nitrile stretch in (APOSS)[$CuCl_{4-x}(SCN)_x$]$_4$ at higher substitution levels of SCN^-. Growth of an additional peak starting at $x = 0.61$ is highlighted.

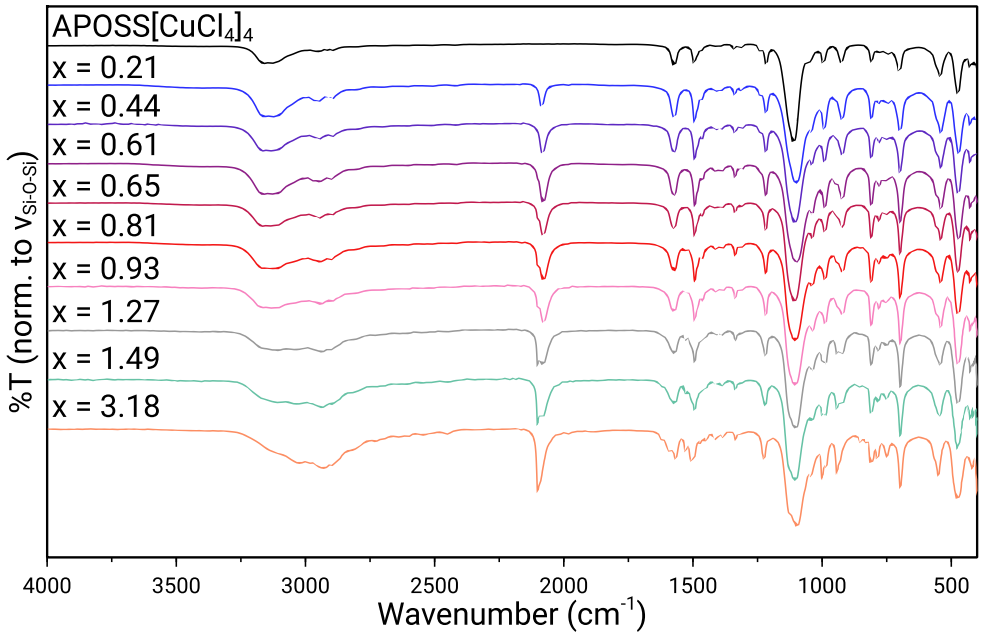

Figure S41. Full FTIR spectra of (APOSS)[$CuCl_{4-x}(SCN)_x$]$_4$ at higher substitution levels of SCN^-.

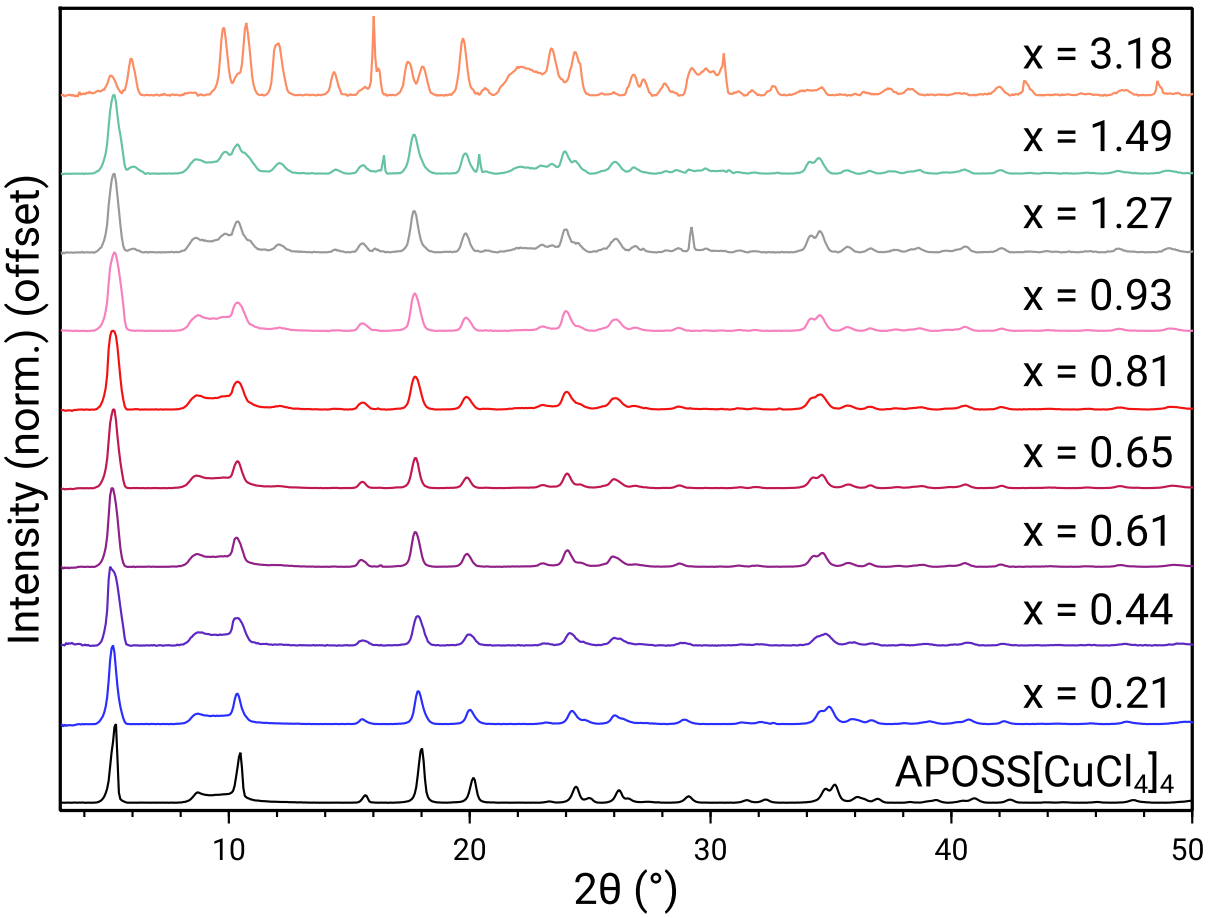

Figure S42. Powder X-ray diffraction patterns of (APOSS)[$CuCl_{4-x}(SCN)_x$]$_4$ at higher substitution levels of SCN^-.

3. Additional Tables

Table S3. Crystal data and structure refinement for (APOSS)[$CuCl_4$]$_4$.

Identification code	2354173	
Empirical formula	C6 H18 Cl4 Cu N2 O3 Si2	
Formula weight	427.74	
Temperature	100(2) K	
Wavelength	0.71073 Å	
Crystal system	Orthorhombic	
Space group	*F*mmm	
Unit cell dimensions	a = 10.2369(6) Å	a= 90°.
	b = 20.4352(12) Å	b= 90°.
	c = 33.981(2) Å	g = 90°.
Volume	7108.6(8) Å^3	
Z	16	
Density (calculated)	1.599 Mg/m^3	
Absorption coefficient	1.965 mm^{-1}	
F(000)	3472	
Crystal size	0.110 x 0.100 x 0.100 mm^3	
Theta range for data collection	1.198 to 25.154°.	
Index ranges	–12<=h<=11, 0<=k<=24, –9<=l<=40	
Reflections collected	3216	
Independent reflections	1734 [R(int) = 0.0302]	
Completeness to theta = 25.000°	97.4 %	
Refinement method	Full-matrix least-squares on F^2	
Data / restraints / parameters	1734 / 42 / 140	
Goodness-of-fit on F^2	1.234	
Final R indices [I>2sigma(I)]	R1 = 0.0790, wR2 = 0.1937	
R indices (all data)	R1 = 0.0826, wR2 = 0.1966	
Largest diff. peak and hole	1.359 and -0.631 e.Å^{-3}	

Table S4. Experimental stretching frequencies of various thiocyanate species

	Cu(SCN)	$Cu(SCN)_2$	NH_4SCN	APOSS[$CuCl_{4-x}(SCN)_x$]$_4$
SCN Stretch (cm^{-1})	2175.5	2151.8	2063.6	2082.0

4. References

(1) J. A. Hunter, W. H. S. Massie, J. Meiklejohn and J. Reid, *Inorg. Nucl. Chem. Letters*, 1969, **5**, 1–4.

(2) M.-C. Gravel, C. Zhang, M. Dinderman and R. M. Laine, *Appl. Organometal. Chem.* 1999, **13**, 329–336.

(3) S. Kataoka, S. Banerjee, A. Kawai, Y. Kamimura, J.-C. Choi, T. Kodaira, K. Sato, and. A. Endo, *J. Am. Chem. Soc.* 2015, **137**, 4158–4163.

(4) G. M. Sheldrick, (**2005**). CELL_NOW. University of Goettingen, Germany.

(5) Bruker (**2007**) APEX2 (Version 2.1-4), SAINT (version 7.34A), SADABS (version 2007/4), BrukerAXS Inc, Madison, Wisconsin, USA.

(6) G. M. Sheldrick, (**2007**). TWINABS. University of Goettingen, Germany.

(7) (a) G. M. Sheldrick, *Acta Cryst*. 2008, **A64**, 112–122. (b) G. M. Sheldrick, *Acta Cryst*. 2015, **A71**, 3–8.

(8) (a) A. Altomare, C. Burla, M. Camalli, G. L. Cascarano, C. Giacovazzo, A. Guagliardi, A. G. G. Moliterni, G. Polidori and R. Spagna, *J. Appl. Crystallogr*. 1999, **32**, 115–119. (b) A. Altomare, G. L. Cascarano, C. Giacovazzo and A. Guagliardi, *J. Appl. Crystallogr*. 1993, **26**, 343–350.

(9) (a) G. M. Sheldrick, (**1997**) SHELXL-97, Program for the Refinement of Crystal Structures. University of Göttingen, Germany. (b) G. M. Sheldrick, *Acta Cryst*. 2015, **C71**, 3–8.

(10) D. Waasmaier and A. Kirfel, *Acta Crystallographica A* 1995, **51**, 416–430.

(11) (a) A. L. Spek, *J. Appl. Crystallogr*. 2003, **36**, 7–13. (b) P. Van der Sluis, A. L. Spek, *Acta Cryst*. 1990, **A46**, 194–201. (c) A. L. Spek, *Acta. Cryst*. 2009, **D65**, 148–155.

(12) L. J. Farrugia, Ortep-3 for Windows. *J. Appl. Crystallogr*. **1997**, *30*, 565.

(13) W. Li, S. Ding, J. Xu, C. Wu, X. Li, L. Qian, H. Chen, X. Zhang, K. Kang and C. Xiang, *ACS Appl. Energy Mater.* 2024, **7**, 1120–1127.